1969

Infrared spectra and vibrational analyses of some dimeric transition metal pentahalides

Richard Roman Smardzewski
Iowa State University

INFRARED SPECTRA AND VIBRATIONAL ANALYSES OF SOME DIMERIC TRANSITION METAL PENTAHALIDES

by

Richard Roman Smardzewski

A Dissertation Submitted to the
Graduate Faculty in Partial Fulfillment of
The Requirements for the Degree of
DOCTOR OF PHILOSOPHY

Major Subject: Inorganic Chemistry

Approved:

Signature was redacted for privacy.

In Charge of Major Work

Signature was redacted for privacy.

Head of Major Department

Signature was redacted for privacy.

Dean of Graduate College

Iowa State University
Ames, Iowa

1969

TABLE OF CONTENTS

INTRODUCTION

In recent years the study of compounds containing bridging halogen atoms has been enlarged tremendously. Halogen bridging is a common structural feature in a number of heavy metal halides and their related compounds. Little is known, however, about the vibrational frequencies of the bonds present in such compounds. There is a significant lack of information concerning vibrational analyses of halogen-bridged systems, and especially concerning comparisons of bond stretching force constants of terminal metal-halogen bonds with those associated with bridged metal-halogen bonds.

A series of compounds which can provide valuable information on the nature of metal-halogen bonding contains the pentahalides of the 4d and 5d transition metals of Groups VB, VIB and VIIB. Since most of these pentahalides possess strong light absorbing characteristics, Raman light scattering studies prove to be difficult. The abundance of absorption bands in their far infrared spectra in the metal-halogen fundamental region of 500-40 $cm.^{-1}$, however, provides ample information regarding their molecular structure.

A prime object of this work was, through a detailed study of the infrared vibrational spectra of these compounds, to elucidate the nature of the terminal metal-halogen and bridged metal-halogen bonds as a function of both the heavy central metal atom and the corresponding halogen.

Review of Previous Work

Synthesis and stability of pentahalides

A number of methods describing the preparation of the anhydrous chlorides, bromides and iodides of niobium(V) and tantalum(V) are presented in a review by Gutmann (1). The simpler methods generally involve direct combination of the elements in an appropriate temperature gradient. Compounds of reasonable purity are obtained in satisfactory yields using this procedure. In certain instances, vacuum resublimation will augment the quality of the product.

With the exception of the pentafluoride, the only other known pentahalide of molybdenum existing in a condensed phase, is the pentachloride. This compound is prepared by several methods (2,3), most of which involve direct chlorination of the metal at moderately high temperatures of 300-400°C.

The preparation of the chlorides and bromides of tungsten (V) is complicated by the fact that upon direct chlorination or bromination of the metal at high temperatures, the resulting pentahalide is not produced in pure form. Depending upon the temperature, varying amounts of hexahalide are also formed (1). The pentachloride of tungsten is usually prepared by either hydrogen (4,5) or phosphorus (6) reduction of the hexachloride at elevated temperatures. Disproportionation of the tetrachloride of tungsten at moderate temperatures will produce

high quality crystalline WCl_5.[1] Tungsten(V) bromide is prepared (7) in satisfactory yields by sublimation, under a dynamic vacuum at temperatures of ca. 250-300°C., of the mixture of WBr_5 and WBr_6, which is obtained from simple bromination of tungsten metal at elevated temperatures. This process involves decomposition of the WBr_6 to produce WBr_5 and Br_2.

A number of methods (8-10) are described for the preparation of anhydrous rhenium(V) chloride. Most of these involve chlorination of very pure rhenium metal at temperatures of the order of 700°C. The product can be further purified by sublimation in a chlorine atmosphere. Rhenium(V) bromide is produced by direct bromination of the pure metal at a temperature of 650°C. (11).

The chlorides, bromides and iodides of pentavalent niobium differ only slightly in their physical properties from the corresponding pentahalides of tantalum. Yellow niobium(V) chloride is slightly less volatile than white tantalum pentachloride (12). Both can be vacuum sublimed without decomposition. The physical properties of the pentahalides of niobium and tantalum are described in detail elsewhere (1). It is sufficient to say that the orange to red pentabromides can be sublimed in vacuo with little or no decomposition (12). The

---

[1]Hogue, R. D., Ames, Iowa. On the preparation of some lower tungsten halides. Private communication. 1968.

black tantalum pentaiodide can be vacuum sublimed, while the brass-colored niobium(V) iodide undergoes extensive decomposition with vaporization, and can only be sublimed in the presence of sufficient iodine pressures to suppress dissociation (13). Stability with respect to dissociation decreases in the order Cl > Br > I.

Molybdenum(V) chloride exists as a black, light sensitive solid at room temperature which can be vacuum sublimed with slight decomposition (2). Dark green WCl_5 and WBr_5 both sublime in vacuo, accompanied by slight traces of disproportionation products. The thermodynamic properties of tungsten(V) chloride and bromide have been recorded in detail elsewhere (14,15,16).

Rhenium(V) chloride undergoes moderate decomposition and disproportionation at temperatures of the order of 150-250°C., and should be sublimed in the presence of a chlorine atmosphere (10). The pentabromide of rhenium is an extremely unstable green solid melting slightly above room temperature (11). At temperatures much higher than ca. 40°C., or in the presence of organic liquids, extensive decomposition of $ReBr_5$ occurs with evolution of bromine.

Structure and bonding in pentahalides

In the vapor state, the pentachlorides of niobium and tantalum have been shown to exist as monomers. In the case of $NbCl_5$, this was demonstrated by the classical work of Balke and

Smith (17). Schäfer and Sibbing have confirmed the monomeric nature of $TaCl_5$ in the gas phase by means of static vapor density measurements (18). Electron diffraction studies (19,20) have indicated that the pentachlorides and pentabromides of niobium and tantalum exist as approximate trigonal bipyramidal monomers in the vapor state. Gaseous molybdenum(V) chloride has also been shown to exist in the form of a trigonal bipyramidal monomer (21,22). In the case of tungsten pentachloride, there is a report (15) indicating that a dimeric W_2Cl_{10} species may exist in appreciable concentrations in the vapor state. Schäfer and Rinke, however, have not confirmed this through mass spectral studies (23), which indicate the presence of predominantly monomeric WCl_5 units in the vapor.

In the condensed phase, a structural determination through single crystal X-ray diffraction techniques has demonstrated that $NbCl_5$ and $TaCl_5$ each contain discrete dimeric units (24). The structure consists of M_2X_{10} dimers with the chlorine atoms forming two octahedra which share a common edge. The metal atoms, which share two bridging chlorine atoms, are distorted slightly away from the centers of the octahedra. In the dimeric molecule, which has D_{2h} point symmetry, there are three non-equivalent metal-chlorine distances. The structure is illustrated in Fig. 1.

Molybdenum(V) chloride has also been shown to exhibit such a structure in the solid state (25). In the case of the

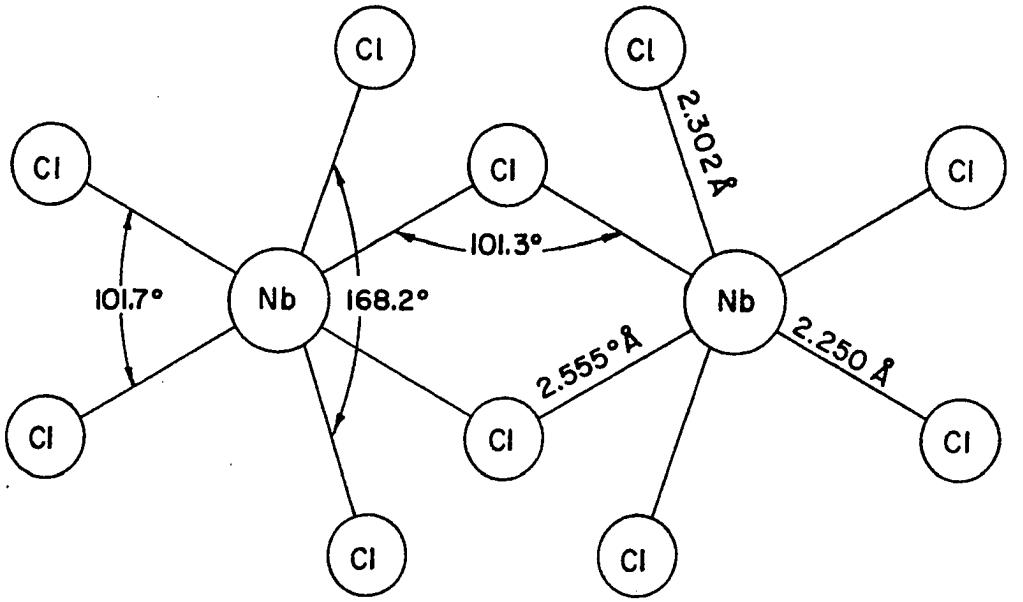

Fig. 1. The Nb_2Cl_{10} structure

solids, WCl_5 and WBr_5, Colton and Tomkins, on the basis of magnetic evidence, had postulated the existence of trinuclear metal clusters (26). According to their description, the tungsten(V) halides are better formulated as $[W_3X_{12}]^{3+}X_3^-$. Boorman et al. (27), however, have demonstrated through single crystal X-ray diffraction that WCl_5 possessed a bridged dimeric structure similar to $NbCl_5$. Tungsten(V) chloride is, in fact, isostructural with molybdenum(V) chloride and has unit cell dimensions within 1% of those for $MoCl_5$.

Uranium(V) chloride, though not isostructural with $NbCl_5$ has been shown to contain discrete U_2Cl_{10} dimeric units in the solid state (28). To date, the latest example of a dimeric halogen-bridged pentahalide is solid rhenium(V) chloride (29). In this case, $ReCl_5$ is neither isostructural with $NbCl_5$ nor UCl_5. These three compounds differ in the packing of the Cl atoms and represent three crystallographically distinct ways of forming M_2Cl_{10} dimers in the solid state.

The magnetic susceptibilities of some dimeric metal pentahalides have been measured. The pentahalides of niobium and tantalum are diamagnetic, as would be expected for a d^0 system. For $MoCl_5$, $\mu_{eff.} = 1.51$ B.M. at 293°K. (30). For WCl_5, $\mu_{eff.} = 1.07$ B.M. at 300°K., and WBr_5 $\mu_{eff.} = 1.05$ B.M. at 300°K. (31). These data would seem to suggest little if any metal-metal interaction in the pentahalides of molybdenum and tungsten. Brown and Colton (9) have determined the magnetic

susceptibility of rhenium pentachloride, for which $\mu_{eff.}$ = 2.57 B.M. at 300°K. Here again, there appears to be no strong metal-metal interaction. Due to its extreme instability, magnetic data is not yet available for rhenium(V) bromide (11). A summary of the structural and magnetic parameters available for some heavy transition metal pentahalides is contained in Table 1.

Relatively little work has been done to elucidate the nature of the metal pentahalides in solution. Kepert and Nyholm (32) have shown that $NbCl_5$ exists as a dimeric non-electrolyte in concentrated solutions of dry, oxygen free, carbon tetrachloride and nitromethane. Werder et al. (33) have demonstrated, by means of infrared studies, that $NbCl_5$ exists predominantly in the dimeric M_2X_{10} form in cyclohexane. In relatively nonpolar solvents the dimeric species is expected to be the more stable form. In unidentate coordinating solvents, adducts of the type $MX_5 \cdot L$ or $MX_4 \cdot L_2$ are usually formed (1,5,34). There is a report (35), based on spectral data, which indicates that $MoCl_5$ is monomeric in cyclohexane. The evidence presented, however, is far from conclusive.

Reddoch (36) has studied the nuclear quadrupole resonance spectra of $NbCl_5$ and $TaCl_5$. A single ^{35}Cl resonance was found for both compounds, indicating one type of Cl atom in the solids. This finding is indeed puzzling and indicates a definite need for further study.

Table 1. Structural and magnetic data of some heavy metal pentahalides

Compound	Phase	d(M-Xt)[a] Å	d(M-Xb)[b] Å	d(M-M)[c] Å	$\mu_{eff.}$ B.M.	Ref.
$NbCl_5$	gas	2.29 ± .03				19
	solid	2.250 ± .006 2.302 ± .005	2.555 ± .006	3.951 ± .002	diamag.	24
$NbBr_5$	gas	2.46 ± .03				19,20
$TaCl_5$	gas	2.30 ± .02				19
$TaBr_5$	gas	2.45 ± .03				19,20
$MoCl_5$	gas	2.27 ± .02				21,22
	solid	2.24 ± .01 2.25 ± .01	2.53 ± .01	3.84 ± .02	1.51[d]	10,25
WCl_5	solid				1.07[e]	31
WBr_5	solid				1.05[e]	31
$ReCl_5$	solid	2.24 ± .01 2.27 ± .01	2.47 ± .01	3.739 ± .002	2.57[e]	9,29
UCl_5	solid	2.43 ± .01 2.44 ± .01	2.70 ± .01	4.165 ± .003		28

[a]Terminal metal-halogen distance.

[b]Bridged metal-halogen distance.

[c]Metal-metal distance.

[d]Measured at 293°K.

[e]Measured at 300°K.

Vibration spectra of pentahalides

In the past there has been considerable confusion concerning the interpretation of the vibrational spectra of the heavier transition metal pentahalides of Groups VB and VIB Gaunt and Ainscough (37) were the first to study in detail the vibrational spectrum of $NbCl_5$ in both the solid state and in CS_2 solution. They interpreted their results on the basis of a trigonal bipyramidal monomer having D_{3h} symmetry. Carlson (38), in the light of X-ray and ultraviolet spectral data (24, 39), did later acknowledge the difficulties of such a model in his interpretation of the Raman and infrared spectra of $NbCl_5$ and $TaCl_5$ in both the solid form, and in CS_2 or CCl_4 solutions. Nevertheless, he proceeded to assign the spectra on the basis of a D_{3h} monomer. This was due, in part, to the wrong choice of symmetry for the M_2X_{10} dimer, viz. C_{2h} rather than D_{2h}, and low quality spectra. Bader and Huang (35), through vibrational spectral studies of cyclohexane and CCl_4 solutions of the pentachlorides of Nb, Ta, Mo and W, concluded that these compounds exist as monomers in solution. In the past, detailed vibrational analyses have even been carried out on the vibrational solution spectra of $NbCl_5$ and $TaCl_5$, using a monomeric model with D_{3h} symmetry (40,41).

Recently Walton and Brisdon (42), through a careful examination of the far infrared spectra of $NbCl_5$, $NbBr_5$, $TaCl_5$, $TaBr_5$ and WCl_5 in the metal-halogen stretching region of

500-200 cm.$^{-1}$, conceded the possibility of these compounds existing as discrete M_2X_{10} dimers in the solid state. Werder et al. (33) have examined the single crystal laser Raman and infrared spectrum of $NbCl_5$ in solid, matrix and solution form. Although their vibrational spectra and frequency assignments were questionable, there was indeed strong evidence to indicate that $NbCl_5$ does exist as a dimer in both the solid state and in saturated cyclohexane and CCl_4 solutions.

Because of these very apparent uncertainties as to the interpretation of the vibrational spectra of the existing crystalline pentachlorides, bromides and iodides of Nb, Ta, Mo, W and Re, this detailed study of their infrared spectra was undertaken. It was also hoped to reveal any correlation between vibrational force constants and the nature of the metal-halogen bonds present in these unusual compounds.

EXPERIMENTAL

Materials

In this work, all of the metal pentahalides were susceptible to air oxidation and hydrolysis, and were contained in evacuated vessels or inert atmospheres during preparation and experimentation. Also these compounds were stored and handled in a dry-box under an argon atmosphere. The dry-box was maintained at a dew point of ca. -60°C. by circulating a constant flow of dry argon throughout the box. All reactions and preparations were carried out in either evacuated Pyrex or Vycor vessels, after the necessary preliminary procedures had been executed in the dry-box and on the vacuum manifold.

Metals

The metals used in the syntheses of the respective pentahalides were in the form of either high purity powders or granules. The niobium metal used in this work was supplied by E. I. duPont de Nemours and Co. in the form of high purity granules. Tantalum powder obtained from the Fansteel Metallurgical Corporation, Metal Products Division, was used in the preparation of all tantalum(V) halides. Tungsten metal was obtained in the form of 200 mesh powder from the Lamp Metals and Components Department of the General Electric Company. Molybdenum metal, in the form of granules, was supplied by the Climax Molybdenum Company. High grade rhenium powder was obtained from the Cleveland Refractory Metals Company, Rhenium

Division. Prior to the preparation of the corresponding pentahalides of tungsten and rhenium, the respective metals were further purified by hydrogen reduction at elevated temperatures.

Halogens

Chlorine was obtained from lecture bottles and used without further purification. The bromine used in these experiments was reagent grade and subsequently purified by refluxing over phosphorus(V) oxide, distilling through outgassed Linde 3A Molecular Sieves, and storing over anhydrous tantalum(V) bromide *in vacuo*. Reagent grade iodine was further purified by grinding the solid with potassium iodide and twice resubliming.

Organic solvents

Cyclohexane was obtained in spectroquality grade from the Matheson, Coleman and Bell Company, refluxed *in vacuo* over phosphorus(V) oxide and subsequently stored over metallic sodium.

Synthesis of Metal Pentahalides

In most cases, the pentahalides of niobium, tantalum, molybdenum, tungsten and rhenium were generally prepared by a direct combination of the elements in an appropriate temperature gradient.

Group VB pentahalides

The chloride, bromide and iodide of niobium(V) were

prepared and made available by Peter B. Fleming (43). The corresponding halides of tantalum(V) were provided by Peter A. Kilty[1]. Essentially, the pentachlorides of niobium and tantalum were prepared in high yield by passing gaseous chlorine over the metal which was maintained at temperatures of 400-450°C. Similarly, in the cases of $NbBr_5$ and $TaBr_5$, gaseous bromine at a pressure of ca. 200 mm. was passed over the metal, which was maintained at temperatures of 400-450°C., to produce the corresponding pentabromide. The pentaiodides of niobium and tantalum were prepared by a direct reaction of the elements in a sealed tube in an iodine/metal temperature gradient of 180°C./450°C.

Group VIB pentahalides

Crystalline molybdenum(V) chloride was made available by John L. Meyer[2]. In this case, gaseous chlorine was passed over molybdenum powder, which was maintained at a temperature of ca. 450°C. to produce the resultant black $MoCl_5$.

The chlorides and bromides of tungsten(V) were prepared, analyzed and made available by Ronald D. Hogue (44). The pentachloride of tungsten was prepared by the disproportionation of the tetrachloride at temperatures of 450-500°C.

---

[1]Kilty, P. A., Ames, Iowa. On the preparation of some tantalum halides. Private communication. 1966.

[2]Meyer, J. L., Ames, Iowa. On the preparation of some mixed molybdenum-tantalum cluster species. Private communication. 1968.

Gaseous bromine at a pressure of 200 mm. was passed over tungsten metal powder, held at a temperature of 500°C., to produce a mixture of WBr_5 and WBr_6. This mixture then was sublimed under a dynamic vacuum at temperatures of ca. 250-300°C. to afford high quality crystalline WBr_5.

Group VIIB pentahalides

Rhenium(V) chloride was prepared in moderate yields by passing gaseous chlorine at a pressure of one atmosphere over freshly hydrogen-reduced rhenium powder, which was held at a temperature of 600°C. The subsequent reaction product was resublimed in a chlorine atmosphere to yield a black crystalline product. A spectrophotometric rhenium analysis (45) of this final product indicated it to be high quality $ReCl_5$. Attempts to prepare the pentabromide of rhenium in reasonable yields were unsuccessful. For a period of ca. one month, gaseous bromine at a pressure of 200 mm. was passed over rhenium powder which was maintained at 750°C. During that time, only slight traces of what appeared to be $ReBr_5$ were produced.

Infrared Spectra

Spectrophotometer

In this work, the infrared absorption spectra of the various metal pentahalides were recorded over the range 800-42.5 $cm.^{-1}$. Spectral measurements were carried out on a double-beam Beckman IR-11 recording spectrophotometer. The instrument utilized four gratings and eight transmission

filters over the entire range of operation. Throughout most of the range, the spectral resolution was 0.5-1 cm^{-1}. Over the entire range, the wavenumber repeatability was 0.5 $cm.^{-1}$ and % T repeatability was 1% plus noise level. The wavenumber accuracy was $\pm$ 1 $cm.^{-1}$ throughout the entire range. In all cases during absorption measurements, the sample compartment of the spectrophotometer was continually purged with dry air and all measurements were recorded with dry air in the reference beam.

Room temperature spectra

At room temperature, infrared absorption measurements were carried out on samples prepared in the form of nujol mulls pressed between two thin polyethylene sheets. The anhydrous compounds were first ground to ca. 200 mesh and then thoroughly mixed with nujol to produce a homogenized mull. The resultant mixture was then pressed between two thin polyethylene sheets and placed in a specially designed tightly sealed sample cell. All operations were executed in an inert atmosphere, where sample preparations were effected immediately prior to infrared spectral measurements. Mulls were found to be air stable over a period of several hours in the cell.

Low temperature spectra

Low temperature infrared absorption measurements in the spectral region of 800-200 $cm.^{-1}$ were carried out on samples using a cryostated matrix isolation cell which had been con-

structed according to a modified design of some ordinary low temperature cells (46,47). Samples of metal pentahalides were vapor deposited through a primary inlet onto an inner CsI cold window which was cooled by a liquid nitrogen reservoir. The inner CsI window temperature was measured by a copper-constantan thermocouple. Indium gaskets were used to provide the necessary thermal contact between the CsI cold window and the copper block housing. The outer cell windows were constructed of polished cesium iodide. A secondary inlet permitted simultaneous deposition of a matrix gas. At deposition temperatures of 85-90°K., cyclohexane proved to be a desirable matrix material because of its high transmittance in the far infrared. In certain cases, it was found that only a slight amount of cyclohexane codeposited with the sample pentahalide was sufficient to greatly improve the spectral resolution in the metal-halogen stretching region of the infrared.

Solution spectra

Infrared absorption studies were carried out on solutions contained in polyethylene molded cells of 1-2 mm. pathlength. These cells were purchased from the Barnes Engineering Company, Instrument Division, Stanford, Connecticut. Preparations and manipulations of the air sensitive solutions were performed in a specially designed solvent dry-box.

RESULTS AND DISCUSSION

Infrared Spectra of Metal Pentahalides

The far infrared absorption spectra of some Group VB, VIB and VIIB transition metal pentahalides are depicted in Figs. 2, 3, 4 and 5. The corresponding band maxima are reported in Tables 2, 3, 4 and 5.

Niobium(V) halides

The infrared absorption spectra of the chloride, bromide and iodide of niobium(V) are illustrated in Fig. 2. In the case of niobium(V) chloride, in order to increase the spectral resolution in the terminal Nb-Cl stretching region, Nb_2Cl_{10} was vapor deposited onto a cold (90°K.) CsI window simultaneously with a known quantity of cyclohexane, thus forming a matrix. The matrix/active species ratio (M/A) was ca. 0.5. The absorption spectrum of this highly concentrated Nb_2Cl_{10} matrix is also represented in Fig. 2. Matrix dilution studies indicated the presence of only the dimeric form of niobium(V) chloride in the concentrated matrix. Werder et al. (33) have observed similar results in their studies of Nb_2Cl_{10} in cyclohexane matrices and in cyclohexane and carbon tetrachloride solutions. Nujol mulls of niobium(V) chloride at room temperature were used to obtain the lower energy portion of the far infrared absorption spectrum of niobium(V) chloride.

Niobium(V) bromide and iodide were prepared in the form of nujol mulls and their absorption spectra in the far infrared

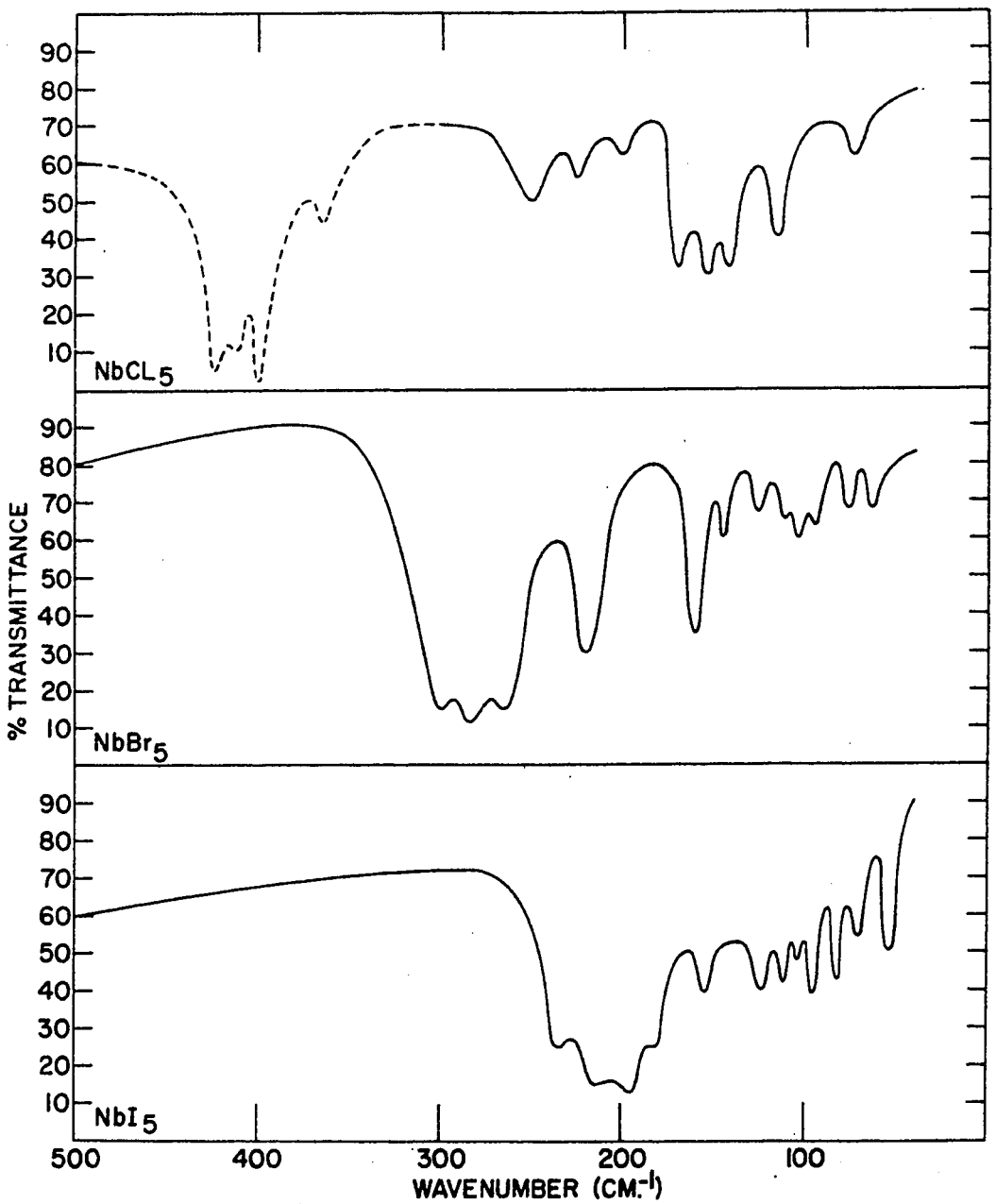

Fig. 2. Far infrared spectra of dimeric NbX_5 (X = Cl, Br, I)
Solid lines represent nujol mulls. The dashed line corresponds to a conc. cyclohexane matrix (M/A ≅ 0.5).

region was measured at room temperature. The results are shown in Fig. 2. The absorption band maxima of the niobium(V) halides are contained in Table 2.

Table 2. Far infrared absorption spectra of the niobium(V) halides

Nb_2Cl_{10} ($cm.^{-1}$)[a]	Nb_2Cl_{10} ($cm.^{-1}$)[b]	Nb_2Br_{10} ($cm.^{-1}$)[a]	Nb_2I_{10} ($cm.^{-1}$)[a]
	423(vs)	299(vs)	233(ms)
	412(vs)	283(vs)	213(s)
400(vs,br)	400(vs)	263(vs)	195(s)
357(ms)	365(s)	219(ms)	184(ms)
251(ms)	251(ms)	159(ms)	153(m)
223(mw)	225(mw)	145(mw)	124(m)
197(mw)		127(mw)	113(m)
171(m)		112(mw)	104(mw)
154(m)		105(mw)	97(m)
142(m)		96(mw)	82(m)
116(m)		77(mw)	71(mw)
73(mw)		63(mw)	54(m)

[a]Nujol mulls. Relative intensities are: s = strong, m = medium, v = very, w = weak, br = broad.

[b]Cyclohexane matrix at 90°K., and M/A $\simeq$ 0.5.

In the infrared spectra of Nb_2X_{10} (X = Cl, Br, I), twelve bands have been observed. The spectra of the niobium(V) halides were quite similar, taking into account the apparent frequency shifts with the corresponding change in halogen atom. In each case, four strong bands designated as $\nu(Nb\text{-}X_T)$ occurred in the terminal niobium-halogen stretching region. Two medium-strong bands, symbolized as $\nu(Nb\text{-}X_B)$, occurred in what may be called the bridged niobium-halogen stretching region of

the infrared. Six absorption bands, designated as δ(Nb-X), were observed in the niobium-halogen bending region. The infrared absorption spectrum of niobium(V) iodide was found to be qualitatively different from the corresponding spectra of Nb_2Cl_{10} and Nb_2Br_{10} with regard to the intensities of certain bands. It is believed that these effects are principally caused by the increased interaction of the various vibrational modes of Nb_2I_{10}.

Tantalum(V) halides

In Fig. 3 are exhibited the infrared absorption spectra of the chloride, bromide and iodide of tantalum(V). In order to improve resolution in the ν(Ta-Cl_T) spectral region, the far infrared absorption spectrum of a concentrated matrix of Ta_2Cl_{10} in cyclohexane (M/A $\cong$ 0.5) was measured at ca. 90°K. Matrix dilution studies over an extended range indicated the presence of only dimeric Ta_2Cl_{10} units in the concentrated matrix. In such a highly concentrated matrix, it was expected that the dimeric form of tantalum(V) chloride would be the predominant species. The matrix spectrum of Ta_2Cl_{10} is also represented in Fig. 3. The remaining low energy portions of the infrared spectrum of tantalum pentachloride were obtained from measurements on nujol mulls at room temperature.

Tantalum(V) bromide and iodide were prepared in the form of nujol mulls and their far infrared absorption spectra are also illustrated in Fig. 3. The corresponding absorption band

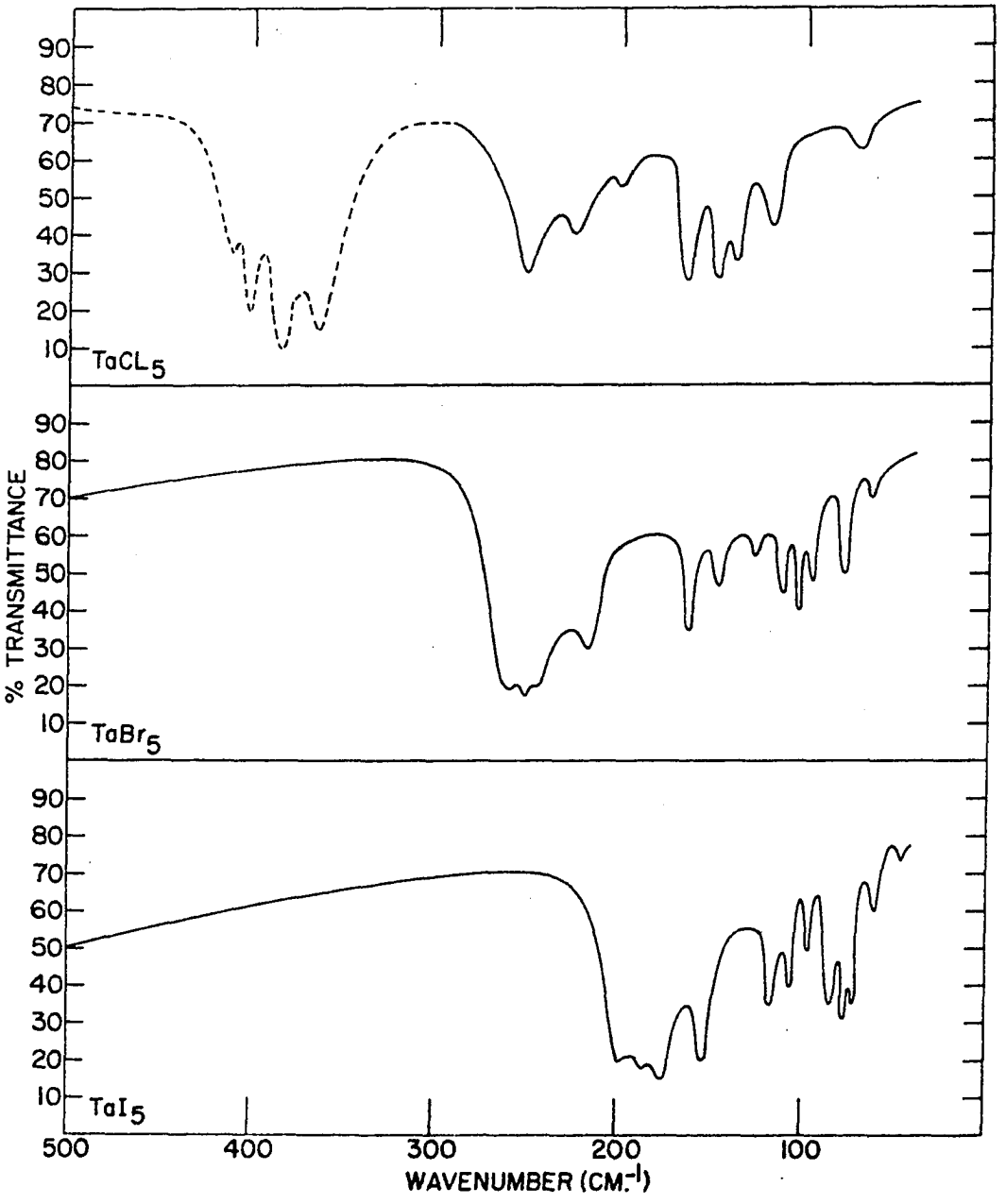

Fig. 3. Far infrared spectra of dimeric TaX_5 (X = Cl, Br, I)
Solid lines represent nujol mulls. The dashed line corresponds to a conc. cyclohexane matrix (M/A ≅ 0.5).

maxima of the compounds Ta_2X_{10} (X = Cl, Br, I) are reported in Table 3.

Table 3. Far infrared absorption spectra of the tantalum(V) halides

Ta_2Cl_{10}		Ta_2Br_{10}	Ta_2I_{10}
$(cm.^{-1})^a$	$(cm.^{-1})^b$	$(cm.^{-1})^a$	$(cm.^{-1})^a$
	411(m)	261(s,sh)	197(s)
	402(vs)	251(s)	186(s,sh)
380(vs,br)	385(vs)	244(s,sh)	176(s)
368(s)	364(s)	217(ms)	155(s)
252(m)	251(m)	162(ms)	116(m)
226(m)	225(m)	147(m)	107(m)
200(mw)		127(w)	95(mw)
164(ms)		112(m)	83(m)
148(ms)		102(ms)	77(m)
138(ms)		96(m)	73(m)
119(m)		79(m)	61(w)
71(mw)		63(w)	45(w)

[a]Nujol mulls. Relative intensities are: s = strong, m = medium, v = very, w = weak, br = broad, sh = shoulder.

[b]Cyclohexane matrix at 90°K., and M/A $\cong$ 0.5.

The infrared absorption spectra of the tantalum(V) halides were quite similar to those obtained for the corresponding niobium(V) halides, both in the number of bands (twelve) and their relative intensities. In the ν(Ta-X_T) region of the spectra of Ta_2X_{10} (X = Cl, Br, I), the band positions were lower in energy than those of the respective niobium(V) halides. This was due, for the most part, to the larger mass of the tantalum atom as compared to that of niobium. The magnitude of the shift to lower frequencies in the

case of the tantalum pentahalides was, however, not entirely due to a mass effect but also reflected a change in the metal-halogen bond force constant.

Tungsten(V) halides

The pentahalides of tungsten, W_2X_{10} (X = Cl, Br), were prepared in the form of nujol mulls and their absorption spectra in the tungsten-halogen fundamental region of the infrared are illustrated in Fig. 4. The infrared spectra of the tungsten(V) halides were strikingly similar to the corresponding spectra of the niobium(V) and tantalum(V) halides. The only major difference occurred in the bridged tungsten-halogen stretching region, where it was observed that the intensities of the two band maxima were the reverse of those observed for the respective niobium and tantalum pentahalides.

In the spectrum of W_2Br_{10}, there was a high frequency band at 329 $cm.^{-1}$ of relatively weak intensity. This band occurred at an extremely high frequency to be a tungsten-bromine stretching fundamental and was therefore considered to be either a combination or an overtone band, possibly activated by Fermi resonance (48). In both spectra of the tungsten(V) halides, there were observed twelve fundamentals in all: $4\nu(W\text{-}X_T)$, $2\nu(W\text{-}X_B)$ and $6\delta(W\text{-}X)$. Absorption band maxima for the tungsten pentahalides studied in this work are listed in Table 4.

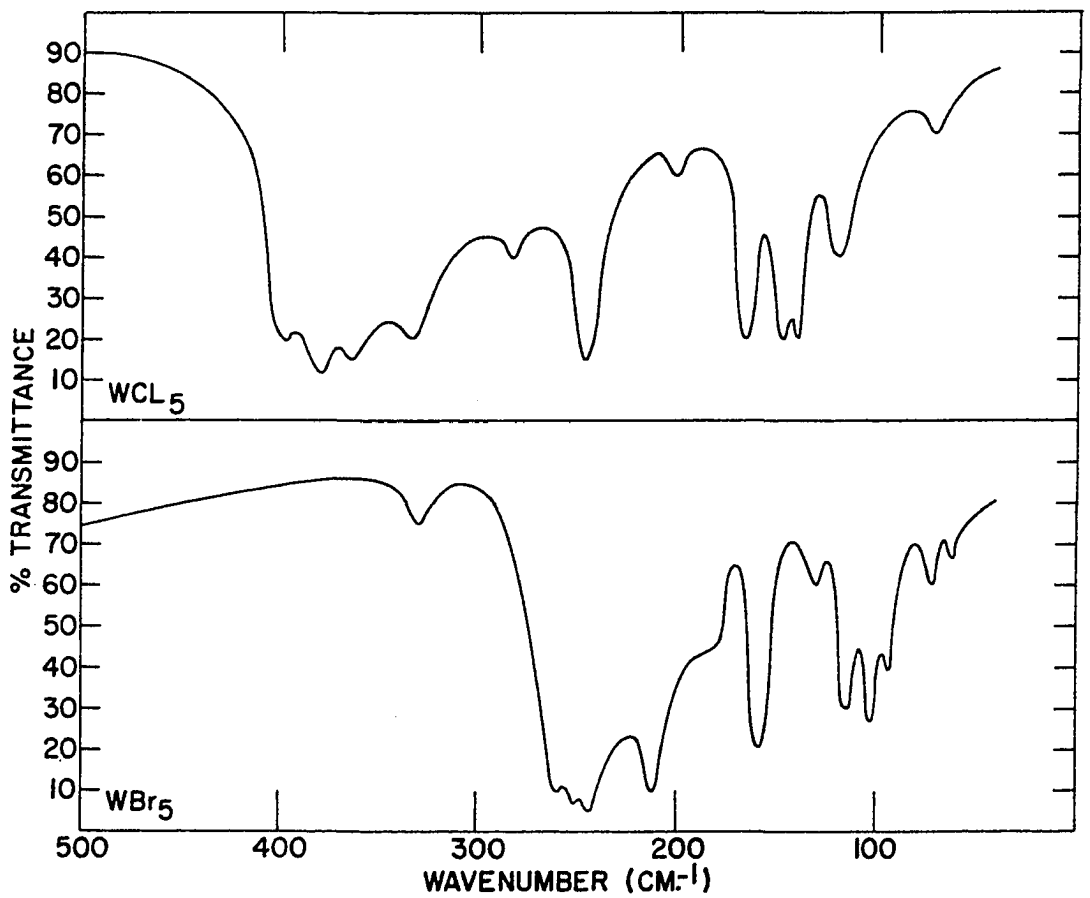

Fig. 4. Far infrared spectra (nujol mulls) of dimeric WX_5 (X = Cl, Br)

Table 4. Far infrared absorption spectra of the tungsten(V) halides

W_2Cl_{10} ($cm.^{-1}$)[a]	W_2Br_{10} ($cm.^{-1}$)[a]
	329(w)
398(s)	260(s)
379(vs)	253(s,sh)
365(vs,sh)	244(s)
334(s)	212(s)
283(mw)	179(m,sh)
247(s)	158(s)
203(w)	129(w)
166(s)	114(ms)
148(s)	103(ms)
141(s)	95(ms)
121(m)	73(w)
72(w)	63(w)

[a]Nujol mulls. Relative intensities are: s = strong, m = medium, v = very, w = weak, sh = shoulder.

Molybdenum(V) and rhenium(V) chlorides

In Fig. 5 are exhibited the infrared absorption spectra of molybdenum(V) chloride and rhenium(V) chloride in the metal-halogen fundamental region. Because of problems involving sample synthesis, it was not possible to obtain the corresponding infrared spectrum of rhenium(V) bromide.

Molybdenum(V) chloride was found to react with nujol. The Mo_2Cl_{10} compound, therefore, was ground to a fine (325 mesh) particle size and the infrared absorption spectrum of the dry powder was subsequently determined. The far infrared spectrum of Mo_2Cl_{10} closely resembled that of W_2Cl_{10}, especially with relation to the relative intensities of the two bands in the

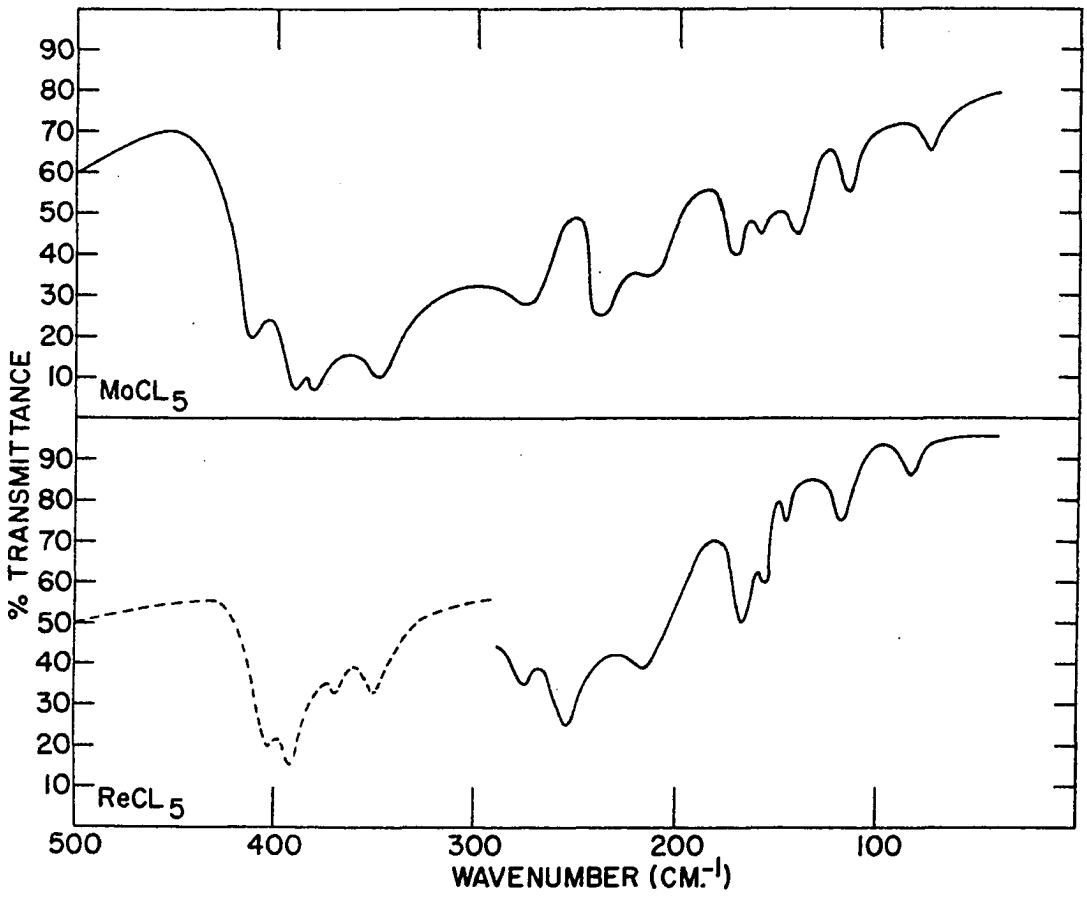

Fig. 5. Far infrared spectra of dimeric MCl_5 (M = Mo, Re)
Solid lines represent solid state spectra. The dashed line corresponds to a satd. cyclohexane solution.

bridged molybdenum-chlorine stretching region.

The infrared absorption spectrum of rhenium(V) chloride had been determined from both nujol mulls and cyclohexane solutions of Re_2Cl_{10}. Because of the slight solubility of Re_2Cl_{10} in cyclohexane, it was possible only to determine accurately the positions of the very intense terminal rhenium-chlorine stretching fundamentals from measurements on solution spectra. Similar band maxima were observed in the terminal Re-Cl stretching region of the nujol mull spectra of solid rhenium(V) chloride thus indicating the stability of dimeric Re_2Cl_{10} units in cyclohexane solution. The less intense bands in the lower frequency spectral region of Re_2Cl_{10} were resolved entirely from nujol mulls. It was noted that the infrared absorption spectrum of rhenium(V) chloride was similar, in all major respects, to the corresponding spectrum of molybdenum(V) chloride. Absorption band maxima for both Mo_2Cl_{10} and Re_2Cl_{10} are reported in Table 5.

Molecular symmetry

The far infrared absorption spectra of all of the transition metal pentahalides studied in this investigation possessed certain dominant characteristics indicative of the molecular symmetry of the metal pentahalides. It was first noted that the infrared absorption spectra of all of these transition metal pentahalides are unusually similar, thus indicating one type of molecular structure. Secondly, in each spectrum there

Table 5. Far infrared absorption spectra of Mo_2Cl_{10} and Re_2Cl_{10}

Mo_2Cl_{10}	Re_2Cl_{10}	
$(cm.^{-1})^a$	$(cm.^{-1})^b$	$(cm.^{-1})^c$
412(ms)	404(s)	405(s)
391(s)	393(s,sh)	388(s)
380(s)	369(ms)	371(ms)
347(s)	350(ms)	347(ms)
276(ms,sh)	276(m)	
238(ms)	255(ms)	
214(m,sh)	216(m,sh)	
172(m)	168(m)	
159(m)	157(mw)	
143(m)	148(mw)	
117(mw)	118(mw)	
75(w)	83(w)	

[a]Powdered (325 mesh) form. Relative intensities are: s = strong, m = medium, w = weak, sh = shoulder.

[b]Nujol mull.

[c]Saturated cyclohexane solution (P.L. = 2 mm.).

were observed twelve metal-halogen fundamentals. Such a large number of fundamentals eliminated the possibility of a D_{3h} trigonal-bipyramidal MX_5 monomeric structure, which can exhibit only five infrared active metal-halogen fundamentals (49). A tetragonal pyramidal MX_5 monomeric molecule having C_{4v} symmetry will exhibit only six metal-halogen fundamentals active in the infrared (50) and was likewise eliminated on that basis.

Vibrational band activation due to crystal site symmetry effects was considered negligible. In the solid state, both

molybdenum(V) chloride and rhenium(V) chloride each contain discrete dimeric M_2Cl_{10} units having approximate D_{2h} molecular symmetry. The solid state structure of molybdenum(V) chloride, however, is considerably different from that of rhenium(V) chloride. The packing mode of the Cl atoms in molybdenum(V) chloride is hexagonal closest packed (25) while that in rhenium(V) chloride is double hexagonal closest packed (29). As is indicated in Fig. 5, however, the infrared absorption spectrum of Mo_2Cl_{10} strongly resembled that of Re_2Cl_{10}, particularly with regard to the relative band intensities. This high degree of spectral correlation of Mo_2Cl_{10} with Re_2Cl_{10} would seem to indicate that the primary features of the infrared absorption spectra of the transition metal pentahalides studied are relatively independent of crystal symmetry effects. The coupling of internal vibrational modes with external crystal modes may cause small but measurable frequency shifts from those expected for the internal vibrations. This coupling, however, will be most prevalent at the lower frequencies (ca. 100 cm^{-1}) which are characteristic of lattice modes. Since in most cases, the majority of the absorption bands of the transition metal pentahalides studied occurred at frequencies higher than ca. 100 $cm.^{-1}$, this type of coupling was considered minor.

The only molecular model which could best represent the infrared data of all of the transition metal pentahalides studied and remain consistent with the previous structural

(24,25,29) and magnetic (9,30,31) data was a dimeric M_2X_{10} molecule having D_{2h} symmetry. According to such a model, thirteen infrared active vibrational modes are predicted: 4 terminal M-X stretches, 2 bridged M-X stretches and 7 M-X bends. In the far infrared spectra of all of the transition metal pentahalides studied, the corresponding vibrations were observed, with the exception of a low frequency bending mode which was believed to lie beyond the range of the spectrophotometer.

Analysis of Vibrations

Observed infrared absorption spectra may be interpreted, through mathematical analyses, in terms of internal structural parameters and bond force constants relating the interactions between bonded and nonbonded pairs of atoms. Since bond force constants qualitatively reflect the strengths of such bonds, one of the prime interests of this study was the evaluation of such force constants in the dimeric M_2X_{10} transition metal pentahalides.

Classical treatment of vibrations

In general, vibrational transitions in a molecule are described most simply by classical mechanics, which yields a solution to the problem of small vibrations which is easier to visualize than the quantum mechanical solution.

The kinetic energy, T, of a molecule having N vibrating

atoms is given by the expression

$$2T = \sum_{\alpha=1}^{N} m_\alpha \left[(d(\Delta x_\alpha)/dt)^2 + (d(\Delta y_\alpha)/dt)^2 + (d(\Delta z_\alpha)/dt)^2 \right] \qquad (1)$$

where m_α is the mass of atom α. When the coordinates Δx_1, Δx_2-----Δz_N are replaced by mass weighted cartesian displacement coordinates, q_1---q_{3N}, defined as $q_1 = m_1^{\frac{1}{2}}\Delta x_1$, $q_2 = m_1^{\frac{1}{2}}\Delta y_1$ ---$q_{3N} = m_N^{\frac{1}{2}}\Delta z_N$, the resultant kinetic energy is expressed as

$$2T = \sum_{i=1}^{3N} \dot{q}_i^{\,2} \qquad (2)$$

where the dot refers to a time derivative.

Since small amplitudes of vibration are assumed, the vibrational potential energy, V, may be expanded in terms of a Taylor series in powers of the displacement coordinates q_i.

$$V = V_o + \sum_{i=1}^{3N} (\partial V/\partial q_i)_o q_i + \tfrac{1}{2} \sum_{i=1}^{3N}\sum_{j=1}^{3N} (\partial^2 V/\partial q_i \partial q_j)_o q_i q_j + 1/3\,! \sum_{i=1}^{3N}\sum_{j=1}^{3N}\sum_{k=1}^{3N} (\partial^3 V/\partial q_i \partial q_j \partial q_k)_o q_i q_j q_k + \text{---} \qquad (3)$$

where the subscript o indicates the evaluation of the derivatives at the equilibrium position. By convention, the potential energy in the equilibrium position, V_o, is equated to zero. Also, since the equilibrium position is characterized by a minimum for the potential energy, all first derivatives are equal to zero. To a first approximation, the anharmonic

terms of third and higher order can be neglected. The reduced expression for the potential energy is then

$$2V = \sum_{i=1}^{3N} \sum_{j=1}^{3N} f_{ij} q_i q_j \qquad (4)$$

where $f_{ij} = f_{ji} = (\partial^2 V/\partial q_i \partial q_j)_o$. Substitution of the expressions for T and V into the Lagrangian equation of motion

$$d/dt(\partial L/\partial \dot{q}_i) - (\partial L/\partial q_i) = 0 \qquad i=1,2---3N \qquad (5)$$

where L = T-V, produces a set of 3N simultaneous, homogeneous linear equations (see Appendix A). These simultaneous equations can be represented by a secular determinant

$$\left| f_{ij} - \lambda \delta_{ij} \right| = 0 \qquad (6)$$

where $\lambda = 4\pi^2 \nu_i^2$ and δ_{ij} is the Kronecker delta symbol.

$$\delta_{ij} = 1 \text{ if } i = j \qquad (7)$$

$$\delta_{ij} = 0 \text{ if } i \neq j \qquad (8)$$

Non trivial solutions of the secular determinant yield frequencies, ν_i, corresponding to the normal modes of vibration. Solutions for these vibrational frequencies, ν_i, will be functions of atomic masses, internal bond distances and angles and the bond force constants.

Only in an extremely few, simple cases is it possible to calculate the force constants, f_{ij}, in a purely theoretical manner. It is generally true that force constants must be evaluated from experimental data. If the geometrical parameters and vibrational frequencies of a molecule are known, it

should be possible to calculate the force constants. Generally speaking, however, there are usually many more force constants than there are experimental frequency data. To overcome this difficulty, it is necessary to neglect some force constants. Consequently, some assumptions must be made as to the form of the force field model used to describe the molecule. There are several types of force fields used (51, 52). One successful model is the generalized valence force field (GVFF). In its simplest form, the generalized valence force field assumes restoring forces opposing changes in valence bonds and changes in the angle between two valence bonds connecting one atom with two others. In other words off-diagonal force constants are neglected.

A generalized valence force field with one off-diagonal term was found to provide quite precise experimental agreement in the cases of the dimeric transition metal pentahalides studied in this investigation.

GF-matrix method

In order to further simplify the analysis of vibrations in a complex polyatomic molecule, a method originally used by Wilson (53,54) is commonly employed. It is generally referred to as the GF-matrix method.

When the vibrations of a polyatomic molecule are expressed in terms of internal coordinates (49,55), the corresponding force constants have a clearer physical meaning than those

expressed in terms of cartesian displacement coordinates. Internal coordinates are strictly defined as coordinates which remain unaffected by translations or rotations of the molecule as a whole. The use of such internal coordinates, therefore, has the effect of reducing the number of coordinates used to describe the molecular vibrations by six in the nonlinear molecule and by five in the linear case. The molecular internal coordinates represent changes in interatomic distances and bond angles (i.e. valence bond angles, twisting angles, torsion angles). A nonlinear polyatomic molecule composed of N atoms will possess 3N-6 independent internal coordinates. The sets of internal coordinates for the M_2X_{10} molecule are illustrated in Fig. 6. Not all of the internal coordinates shown, however, are independent.

In a nonlinear molecule of N atoms, the potential (V) and kinetic (T) energies of vibration can be expressed as functions of the internal coordinates in matrix form as

$$2V = R^T F R \tag{9}$$

$$2T = \dot{R}^T G^{-1} \dot{R} \tag{10}$$

where R represents a column vector of 3N-6 independent internal displacement coordinates while F represents the symmetric force constant matrix of dimension 3N-6, and G is a symmetric matrix containing the molecular parameters (atomic masses, bond distances, etc.). The relationship of the G matrix to the potential energy is demonstrated in Appendix B.

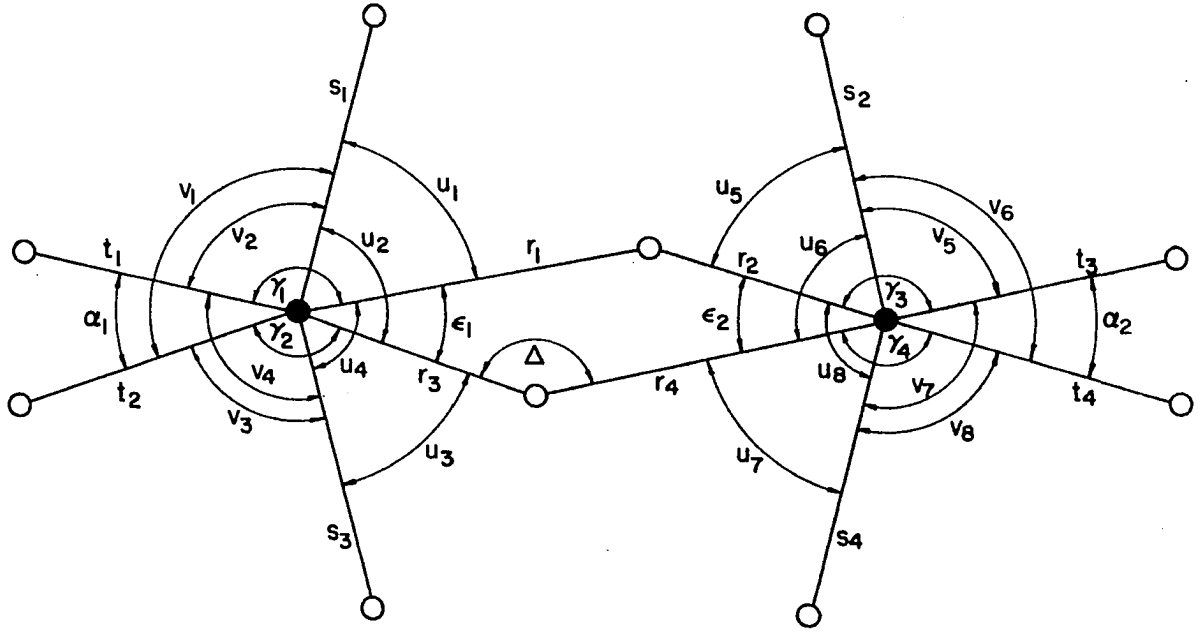

Fig. 6. Internal coordinates of M_2X_{10}

To further extend the treatment of molecular vibrations, the concept of normal coordinates must be included. The normal coordinates, Q_k, represent linear combinations of mass weighted cartesian displacement coordinates, q_k, and one normal coordinate is associated with each normal vibrational mode and vice versa (see Appendix C). Since internal coordinates are related to cartesian displacement coordinates by a linear transformation matrix (Appendix B), normal coordinates are linearly related to the internal coordinates, R_k, and likewise the converse is also true.

$$R = LQ \tag{11}$$

Q is a column vector of normal coordinates (Q_1, Q_2, Q_3---Q_{3N-6}) and L is a transformation matrix of dimension 3N-6. Substituting this relationship into Equations (9) and (10), the potential and kinetic energies are expressed in terms of the normal coordinates.

$$2V = Q^T L^T F L Q \tag{12}$$

$$2T = \dot{Q} L^T G^{-1} L \dot{Q} \tag{13}$$

The definition of the normal coordinates (see Appendix C) is, however, expressed as

$$2V = Q^T \Lambda Q \tag{14}$$

$$2T = \dot{Q}^T E \dot{Q} \tag{15}$$

where E is the identity matrix and $\Lambda = \text{diag}(4\pi^2 \nu_i^2)$. Comparing matrix Equations (12) and (13) with Equations (14) and (15), it is obvious that

$$L^{T}FL = \Lambda \tag{16}$$

$$L^{T}G^{-1}L = E \tag{17}$$

From Equations (16) and (17) is derived the matrix form of the characteristic molecular vibration equation, expressed in terms of the internal coordinates.

$$(GF)L = L\Lambda \tag{18}$$

In this last expression, it can be seen that the frequency parameters expressed in the diagonal Λ matrix are eigenvalues of the GF matrix. Correspondingly, the columns of the L matrix are eigenvectors of the GF matrix and each is related to a particular eigenvalue. The determination of the normal frequencies, normal modes and normal coordinates depends upon the solution of just such a characteristic equation.

Symmetry factoring

In Equation (18) the order of the F and G matrices is often large when the basis coordinates are internal coordinates. It is possible to factor the F and G matrices by transforming to a different set of coordinates. Such a set of coordinates which allows the characteristic vibration equation to be factored to the maximum extent made possible by the symmetry are called the symmetry coordinates (56). One of the most useful types of symmetry coordinates and also that type used in this study are the internal symmetry coordinates (57). Internal symmetry coordinates, S_i, are constructed from appropriate linear combinations of internal coordinates, R_i. This

process can be represented in matrix form as

$$S = UR \tag{19}$$

where $S = \text{col}(S_i)$, $R = \text{col}(R_i)$ and U is the transformation matrix. Methods for constructing such symmetry coordinates are presented elsewhere (58,59,60). It is simply sufficient to state that the internal symmetry coordinates are appropriately chosen linear combinations of equivalent internal coordinates (i.e. internal coordinates which are exchanged by the symmetry operation of the molecule). The internal symmetry coordinates of the M_2X_{10} molecule, along with the related redundancy conditions, are reported in Table 6.

Using group theory (48), the reducible representation for the molecular vibrations of the M_2X_{10} molecule of D_{2h} symmetry, is

$$\Gamma_{vib} = 6A_g+4B_{1g}+2B_{2g}+3B_{3g}+2A_u+4B_{1u}+5B_{2u}+4B_{3u} \tag{20}$$

Upon employing the rules for determining the various vibrational activities (60), it was found that

$$\Gamma(\text{Raman}) = 6A_g+4B_{1g}+2B_{2g}+3B_{3g} \tag{21}$$

$$\Gamma(\text{Infrared}) = 4B_{1u}+5B_{2u}+4B_{3u} \tag{22}$$

$$\Gamma(\text{Inactive}) = 2A_u \tag{23}$$

For the M_2X_{10} molecule, therefore, there are fifteen allowed Raman vibrations and thirteen allowed infrared vibrations. With regard to the infrared allowed vibrations, it can be seen that there are 4 of B_{1u} symmetry, 5 of B_{2u} symmetry and 4 having B_{3u} symmetry. Since this study was concerned only

Table 6. M_2X_{10} symmetry coordinates - infrared

B_{1u}	$S_1 = 1/2(s_1+s_2-s_3-s_4)$
	$S_2 = 8^{-\frac{1}{2}}(v_1+v_2-v_3-v_4+v_5+v_6-v_7-v_8)$
	$S_3 = 8^{-\frac{1}{2}}(u_1+u_2-u_3-u_4+u_5+u_6-u_7-u_8)$
	$S_4 = \Delta$
B_{2u}	$S_5 = 1/2(t_1+t_2-t_3-t_4)$
	$S_6 = 1/2(s_1-s_2+s_3-s_4)$
	$S_7 = 1/2(r_1-r_2+r_3-r_4)$
	$S_8 = 2^{-\frac{1}{2}}(\alpha_1-\alpha_2)$
	$S_9 = 8^{-\frac{1}{2}}(u_1+u_2+u_3+u_4-u_5-u_6-u_7-u_8)$
	$S_{10} = 8^{-\frac{1}{2}}(v_1+v_2+v_3+v_4-v_5-v_6-v_7-v_8)$
	$S_{11} = 1/2(\gamma_1+\gamma_2-\gamma_3-\gamma_4)$
	$S_{12} = 2^{-\frac{1}{2}}(\epsilon_1-\epsilon_2)$
B_{3u}	$S_{13} = 1/2(t_1-t_2+t_3-t_4)$
	$S_{14} = 1/2(\gamma_1+\gamma_2-\gamma_3-\gamma_4)$
	$S_{15} = 8^{-\frac{1}{2}}(u_1-u_2-u_3+u_4+u_5-u_6-u_7+u_8)$
	$S_{16} = 8^{-\frac{1}{2}}(v_1-v_2+v_3-v_4-v_5+v_6-v_7+v_8)$
	$S_{17} = 1/2(\gamma_1-\gamma_2+\gamma_3-\gamma_4)$
	Redundancy conditions
B_{2u}	$S_9 + S_{10} = 0$
	$S_{11} + 2^{-\frac{1}{2}}S_8 + 2^{-\frac{1}{2}}S_{12} = 0$
	$S_{12} = 0$
B_{3u}	$S_{15} + S_{16} = 0$

with the infrared allowed vibrations of the M_2X_{10} molecule, the Raman vibrations will be omitted from further discussion.

With a knowledge of the symmetries of the infrared allowed vibrations in the M_2X_{10} species, it then becomes possible to use the related internal symmetry coordinates to factor the original F and G matrices to yield new F' and G' matrices.

$$(G'F')L' = L'\Lambda \tag{24}$$

For the infrared allowed vibrations of the M_2X_{10} molecule, the orders of the various submatrices contained in F' and G' are 4x4, 5x5, and 4x4. It is shown in Appendix D that

$$F' = UFU^T \tag{25}$$

$$G' = UGU^T \tag{26}$$

and L' represents the linear transformation matrix between the normal coordinates, Q_k, and the internal symmetry coordinates, S_k.

$$S = L'Q \tag{27}$$

Using Equation (24), it is possible to work on each of the factored submatrices separately and therefore the various matrix operations involved in a mathematical vibrational analysis are considerably simplified.

Normal modes of M_2X_{10}

The normal modes of vibration are represented by the normal coordinates. It is difficult, however, to calculate the normal coordinate matrix, Q, prior to a complete vibra-

tional analysis. An exact calculation of the normal coordinates would necessitate a solution of the L' matrix, expressed in Equation (27), and would therefore mean that the characteristic matrix Equation (24) be solved for both eigenvalues, Λ, and eigenvectors, L'. Since this is not possible prior to a complete vibrational analysis, the L' matrix is usually approximated by a unit matrix E. This means that, to a first crude approximation, the normal modes of vibration can be represented by the internal symmetry coordinates, S_k. An approximate description of the infrared active normal vibrational modes of the M_2X_{10} molecule is illustrated in schematic fashion in Fig. 7.

In Fig. 7 it can be seen that the vibrational mode represented as $\nu_4(B_{1u})$ is an out of plane ring bending of the heavy MX_4 units. It is believed that the vibrational energy associated with this type of mode would be extremely low. It was therefore postulated that the frequency of vibration associated with $\nu_4(B_{1u})$ lies at a value lower than the lowest detectable frequency limit (42.5 $cm.^{-1}$) of the infrared spectrophotometer. The out of plane ring bending vibration is usually considered to be the vibrational mode of lowest frequency in dimeric molecules having symmetrically di-bridged systems. Such a vibration is the lowest bending fundamental observed for B_2H_6 and lies at 368 $cm.^{-1}$ whereas the next lowest bending fundamental of diborane lies at 820 $cm.^{-1}$ (61).

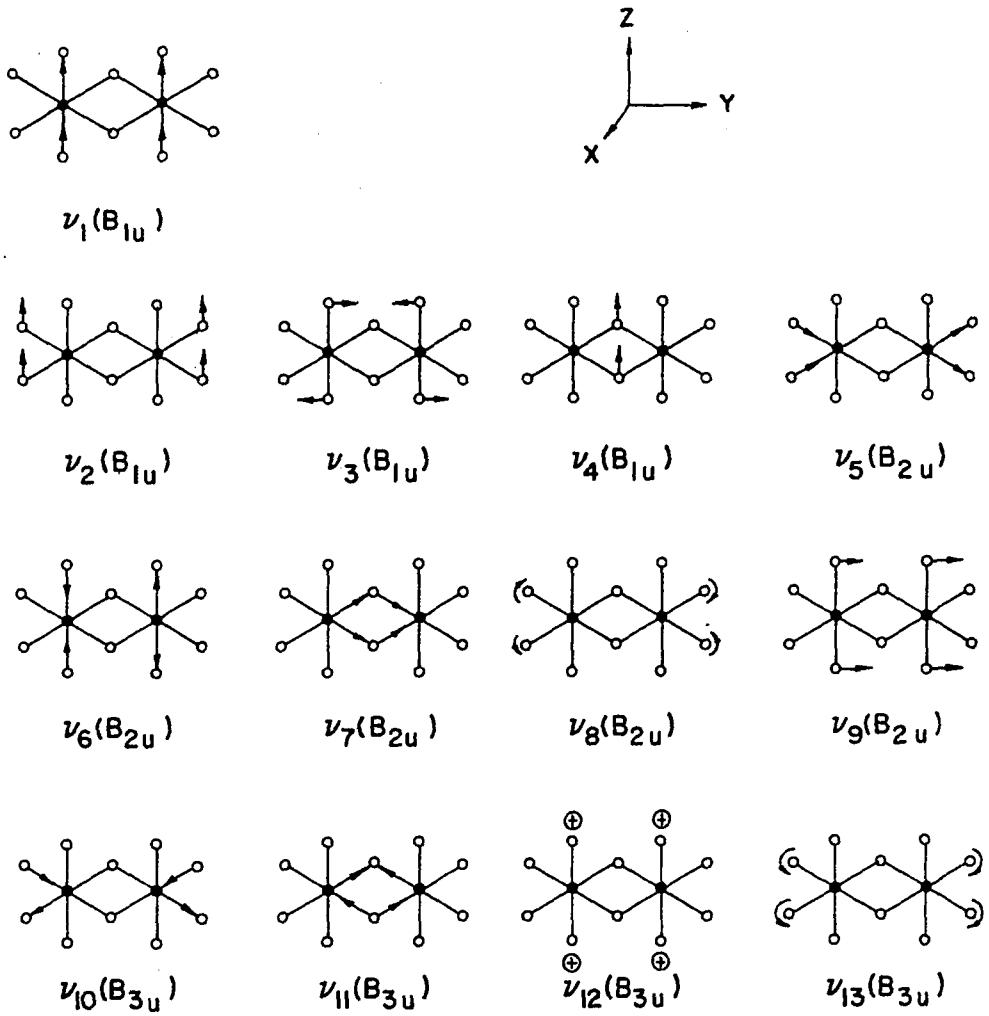

Fig. 7. Vibrational modes (infrared active) of M_2X_{10}

Onishi and Shimanouchi (62) have calculated the nonplanar ring bending mode of Al_2Cl_6 to occur at a frequency of 70 $cm.^{-1}$, some 100 $cm.^{-1}$ below the second lowest infrared active bending fundamental of 170 $cm.^{-1}$. With more massive molecules, this type of vibration has remained undetected. Beattie et al. (63) have not observed the out of plane ring bending mode in the infrared spectrum of Ga_2Cl_6. Similarly, Adams et al. (64) have not observed the out of plane MX_2M ring bending mode in the infrared absorption spectra of the planar molecular anions $[M_2X_6]^{2-}$ (M = Pd, Pt; X = Cl, Br, I). It has also been recently reported that the ring deformation mode has not been observed in the compounds: Au_2Cl_6, Al_2Br_6, Al_2I_6 and In_2I_6 (65). For these reasons, it was therefore postulated that the only remaining unobserved infrared active fundamental of the M_2X_{10} dimeric heavy transition metal pentahalides was $\nu_4(B_{1u})$. For purposes of calculation, the frequency associated with the $\nu_4(B_{1u})$ mode was equated to zero. Consequently, the force constant associated with this type of vibration is equal to zero and the corresponding rows and columns of the F' and G' matrices were omitted. This had the effect of reducing the order of the B_{1u} submatrices of F' and G' by one. This type of reduction of the degree of the characteristic vibrational equation is commonly known as the low frequency approximation (60).

Molecular parameters of M_2X_{10} molecules

In order to calculate force constants for the dimeric transition metal pentahalides, it was first necessary to evaluate their individual G' matrices. The G' matrix contains terms related to the molecular parameters such as atomic masses, bond distances and bond angles. Consequently, a knowledge of the various molecular parameters was a necessary prerequisite to a detailed normal coordinate analysis. Along with the atomic masses, six molecular parameters (3 bond distances and 3 bond angles) were necessary to describe the M_2X_{10} molecules. These quantities, along with a description, are presented in Table 7. In the case of the dimeric pentachlorides M_2Cl_{10} (M = Nb, Ta, Mo, W, Re), the various values for the molecular bond distances and bond angles were known from previously published X-ray structural studies (24,25,27, 29). There were, however, no available structural data for the solid transition metal pentabromides (M_2Br_{10}; M = Nb, Ta, W) and pentaiodides (M_2I_{10}; M = Nb, Ta). For these reasons, certain assumptions had to be made regarding the molecular structures of these compounds.

For the dimeric pentabromides of niobium and tantalum, it was assumed that the terminal metal-bromine distances were equal to those values calculated for the gaseous MBr_5 monomers from electron diffraction studies (19,20). This assumption appeared to be a valid one. In Table 1, it was seen that

Table 7. Molecular parameters of M_2X_{10} halides

Compound	t[a] Å	s[b] Å	r[c] Å	α[d] deg.	β[e] deg.	ε[f] deg.	Ref.
Nb_2Cl_{10}	2.250	2.302	2.555	101.7	168.2	101.3	(24)
Nb_2Br_{10}	2.45	2.45	2.72	101.7	168.2	101.3	text
Nb_2I_{10}	2.61	2.61	2.90	101.7	168.2	89.0	text
Ta_2Cl_{10}	2.250	2.302	2.555	101.7	168.2	101.3	(24)
Ta_2Br_{10}	2.44	2.44	2.71	101.7	168.2	101.3	text
Ta_2I_{10}	2.61	2.61	2.90	101.7	168.2	89.0	text
Mo_2Cl_{10}	2.24	2.24	2.53	96.4	167.2	98.6	(25)
W_2Cl_{10}	2.24	2.24	2.53	96.4	167.2	98.6	(27)
W_2Br_{10}	2.39	2.39	2.70	96.4	167.2	98.6	text
Re_2Cl_{10}	2.24	2.24	2.47	96.4	170.4	98.6	(29)

[a] t = M-X (equat.) distance.

[b] s = M-X (axial) distance.

[c] r = M-X (bridge) distance.

[d] α = X (equat.)-M-X (equat.) angle.

[e] β = X (axial)-M-X (axial) angle

[f] ε = M-X (bridge)-M angle.

there is little difference between the terminal metal-chlorine distances observed in the gaseous monomers and the solid dimers of niobium(V) and tantalum(V) chloride. This relationship was therefore assumed to hold for the pentabromides of niobium and tantalum. Bridging metal-bromine distances in

Nb_2Br_{10} and Ta_2Br_{10} were calculated by assuming that the distance ratio $d(M\text{-}X_B)/d(M\text{-}X_T)$ was equivalent to that observed in the corresponding pentachlorides. Bond angles in the dimeric pentabromides of niobium and tantalum were set equal to those observed for the Nb_2Cl_{10} molecule (24).

In the dimeric tungsten(V) bromide, the terminal tungsten-bromine distances were calculated from the sum of the covalent radius of bromine (66) and the radius of W(V) as determined from W_2Cl_{10} (27). Bridging metal-bromine distances in W_2Br_{10} were calculated by assuming the distance ratio $d(W\text{-}X_B)/d(W\text{-}X_T)$ was equal to that observed for W_2Cl_{10}. Bond angles in the dimeric tungsten(V) bromide were assumed equivalent to the published values of Mo_2Cl_{10} (25).

No structural data, whatever, were available for the iodides of niobium(V) and tantalum(V). In light of the structural data for the solid pentachlorides of niobium and tantalum (24), the molecules Nb_2I_{10} and Ta_2I_{10} were considered isostructural. Terminal metal-iodine distances were calculated from the sum of the covalent radius of iodine (66) and the covalent radii of Nb(V) and Ta(V) as determined from the structural data (19,24). The bridged metal-iodine distance was calculated on the basis that the distance ratio $d(M\text{-}I_B)/d(M\text{-}I_T)$ was assumed equal to that value observed for the dimeric niobium and tantalum pentachlorides. The bond angles, α and β, in the dimeric niobium(V) and tantalum(V) iodides

were set equal to those observed in the niobium(V) chloride. The bond angle ε was chosen to have a smaller value of 89.0°. This value permitted the bridging iodines in M_2I_{10} (M = Nb, Ta) to remain a distance apart equal to twice the van der Waals radius of iodine, thus remaining sterically unhindered.

Force field of M_2X_{10} molecule

The force field model chosen to describe the infrared allowed vibrations of the dimeric M_2X_{10} transition metal pentahalides was a generalized valence force field with one off-diagonal element. This force field is illustrated in Fig. 8. The simple valence force constants f_s, f_T, f_R, f_α, f_u, f_v, and f_γ are self-explanatory. The force constant designated as f'_{ss} is the interaction force constant of the axial-terminal M-X bonds. In certain cases, f'_{ss} was found to have appreciable values. The only off-diagonal constant, $f_{R\gamma}$, represents the interaction constant between the stretching, Δr, of the M-X bridge and the bending, $\Delta\gamma$, of the X(equatorial-terminal)-M-X (bridge) angle. It was initially thought that such an off-diagonal force constant would have appreciable values since any bridge stretching mode would, of necessity, involve deformation of this angle. Resultant computations, however, indicated that the force constant $f_{R\gamma}$ was negligible in most cases. Nevertheless, the calculated values of $f_{R\gamma}$ did provide a comparison check of the magnitudes of the off-diagonal and diagonal force constants, thereby indicating the relative

$$2V = \sum_{i=1}^{4} f_{ss}(\Delta s_i)^2 + \sum_{i=1}^{4} f_T(\Delta t_i)^2 +$$

$$\sum_{i=1}^{4} f_R(\Delta r_i)^2 + \sum_{i=1}^{2} f_\alpha t_o^2(\Delta\alpha_i)^2 +$$

$$\sum_{i=1}^{8} f_u s_o r_o(\Delta u_i)^2 + \sum_{i=1}^{8} f_v s_o t_o(\Delta v_i)^2 +$$

$$\sum_{i=1}^{4} f_\gamma t_o r_o(\Delta\gamma_i)^2 + 2 \sum_{i}^{2} \sum_{\substack{j \\ i\neq j}}^{2} f'_{ss}(\Delta s_i \Delta s_j) +$$

$$\sum_{i=1}^{4} f_{R\gamma} r_o(\Delta r_i \Delta\gamma_i)$$

Fig. 8. Force field of M_2X_{10}

importance of the interaction terms. It was concluded that the off-diagonal force constants play an increasingly important role in the cases of the heavier bromides and iodides of the pentavalent transition metals.

Factored characteristic vibrational equation of M_2X_{10}

The final form of the symmetry factored F' matrix, after the elimination of certain redundant symmetry coordinates (67,68), is illustrated in Fig. 9. For the case of the observed infrared fundamentals of M_2X_{10}, it was observed that symmetry factoring had the effect of reducing a 12x12 matrix into a 3x3, a 5x5, and a 4x4 matrix, each of which was operated on separately.

Using certain geometrical methods described in detail elsewhere (69,70), it was possible to compute the unfactored general elements, g_{ij}, of the kinetic energy matrix. For the specific case of the M_2X_{10} molecule of D_{2h} symmetry, these g-elements are represented in Appendix E. A corresponding symmetry factored G' matrix was constructed from the related g-elements. The elements of the factored G' matrix are appropriately chosen linear combinations of the unfactored g-elements. These matrix elements of the symmetry factored kinetic energy matrix, G', are contained in Table 8.

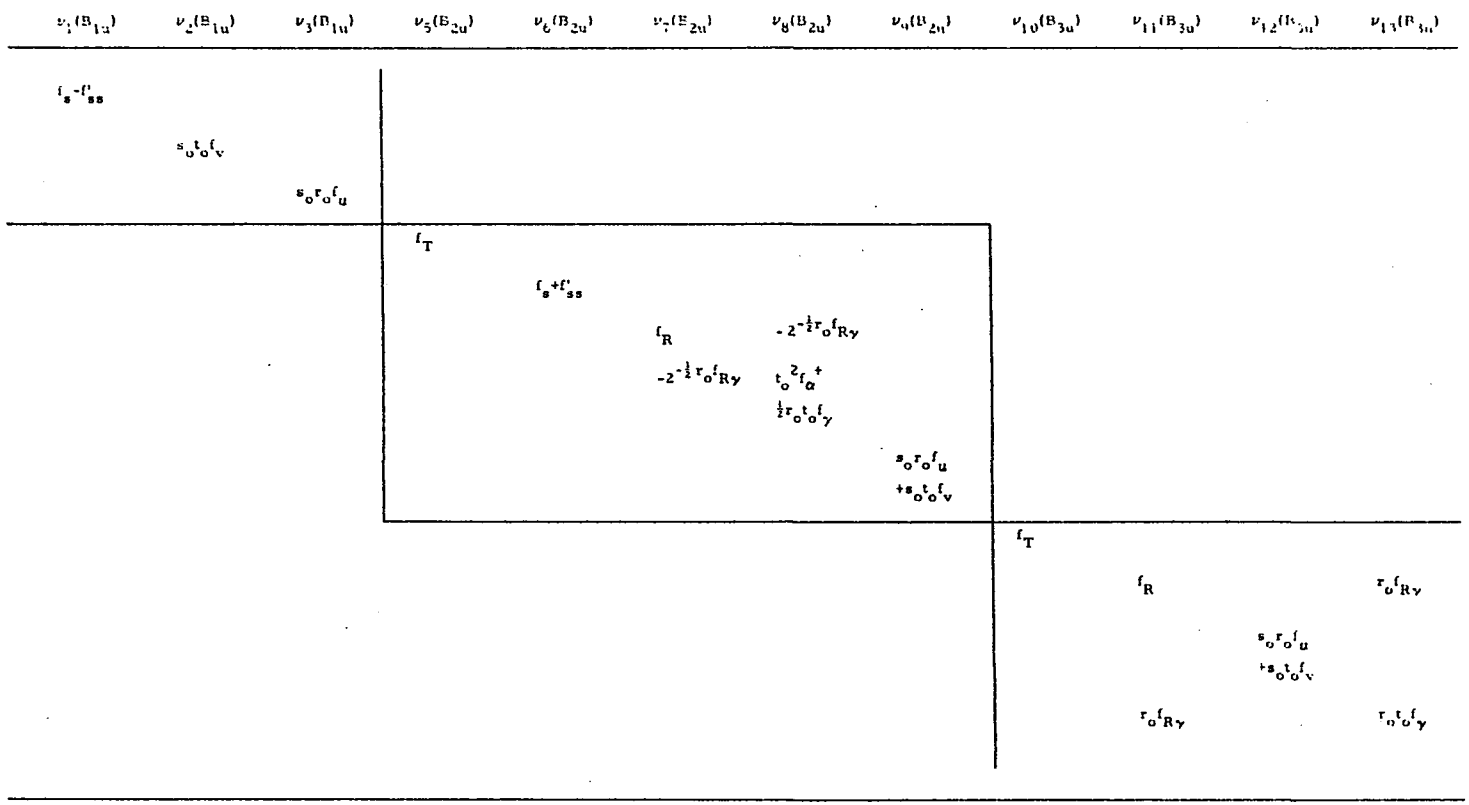

Fig. 9. Symmetry factored F' matrix

Table 8. G' matrix elements of M_2X_{10}

$G'_{11}(B_{1u}) = g_{ss}-g'_{ss}$

$G'_{12}(B_{1u})^a = 2^{\frac{1}{2}}(g_{sv}-g'_{sv})$

$G'_{13}(B_{1u}) = 2^{\frac{1}{2}}(g_{su}-g'_{su})$

$G'_{22}(B_{1u}) = g_{vv} + g'_{vv}-g''_{vv}-g'''_{vv}$

$G'_{23}(B_{1u}) = g_{uv}+g'_{uv}-g''_{uv}-g'''_{uv}$

$G'_{33}(B_{1u}) = g_{uu}+g'_{uu}-g''_{uu}-g'''_{uu}+g^{IV}_{uu}-g^{V}_{uu}$

$G'_{55}(B_{2u}) = g_{tt}+g'_{tt}$

$G'_{56}(B_{2u}) = 2g_{st}$

$G'_{57}(B_{2u}) = g_{tr}+g'_{tr}$

$G'_{58}(B_{2u}) = 2^{\frac{1}{2}}g_{t\alpha}$

$G'_{59}(B_{2u}) = 2^{\frac{1}{2}}(g_{tu}+g'_{tu})$

$G'_{66}(B_{2u}) = g_{ss}+g'_{ss}$

$G'_{67}(B_{2u}) = 2g_{sr}$

$G'_{68}(B_{2u}) = 2^{\frac{1}{2}}g_{s\alpha}$

$G'_{69}(B_{2u}) = 2^{\frac{1}{2}}(g_{su}+g'_{su})$

$G'_{77}(B_{2u}) = g_{rr}-g'_{rr}+g''_{rr}$

$G'_{78}(B_{2u}) = 2^{\frac{1}{2}}g_{r\alpha}$

$G'_{79}(B_{2u}) = 2^{\frac{1}{2}}(g_{ru}+g'_{ru}-g''_{ru})$

$G'_{88}(B_{2u}) = g_{\alpha\alpha}$

$G'_{89}(B_{2u}) = 2g_{\alpha u}$

$G'_{99}(B_{2u}) = g_{uu}+g'_{uu}+g''_{uu}+g'''_{uu}-g^{IV}_{uu}-g^{V}_{uu}$

[a] $G'_{ab} = G'_{ba}$.

Table 8. (Continued)

$$G'_{10,10}(B_{3u}) = g_{tt}-g'_{tt}$$
$$G'_{10,11}(B_{3u}) = g_{tr}-g'_{tr}$$
$$G'_{10,12}(B_{3u}) = 2^{\frac{1}{2}}(g_{tu}-g'_{tu})$$
$$G'_{10,13}(B_{3u}) = g_{t\gamma}-g'_{t\gamma}$$
$$G'_{11,11}(B_{3u}) = g_{rr}+g'_{rr}-g''_{rr}$$
$$G'_{11,12}(B_{3u}) = 2^{\frac{1}{2}}(g_{ru}-g'_{ru}+g''_{ru})$$
$$G'_{11,13}(B_{3u}) = g_{r\gamma}-g'_{r\gamma}+g''_{r\gamma}$$
$$G'_{12,12}(B_{3u}) = g_{uu}-g'_{uu}-g''_{uu}+g'''_{uu}+g^{IV}_{uu}+g^{V}_{uu}$$
$$G'_{12,13}(B_{3u}) = 2^{\frac{1}{2}}(g_{\gamma u}-g'_{\gamma u}+g''_{\gamma u})$$
$$G'_{13,13}(B_{3u}) = g_{\gamma\gamma}-g'_{\gamma\gamma}+g''_{\gamma\gamma}$$

Refinement of Force Constants

Least squares refinement procedure

The least squares force constant refinement procedure used in this study was based on the original method of Mann et al. (71,72) with some modifications. The method itself consists of a regression analysis in which a quantity relating the calculated and experimental observables is minimized. Initially, a trial set of force constants, f_m, was chosen. These trial force constants were then used to calculate a set of vibration frequencies, υ_n, and the Jacobian matrix elements of those frequencies with respect to all the force constants ($\partial \upsilon_n/\partial f_m$). This Jacobian matrix was then used to

set up linear equations for the changes to be made in the trial force constants in order to improve agreement between the observed and calculated frequencies. The linear equations were solved by the method of least squares. The whole process was repeated with successively improved sets of force constants until no further linear refinement of the constants could be found to improve the agreement between the observed and calculated fundamental frequencies. When this stage is reached, the final iterated force constants are said to comprise the "best set" which provides the best fit of the frequency data.

The quantity used in the minimization procedure is called the variance. The variance, Var(i), is related to the frequency difference between the i+1th calculated set of fundamentals, υ_n^{i+1}, and the observed fundamentals, υ_n^o. The variance is represented as

$$\mathrm{Var}(i) = \sum_{n=1}^{s} \left[(\upsilon_n^{i+1} - \upsilon_n^o)/\upsilon_n^o \right]^2 \qquad (28)$$

where s = number of fundamentals and i = iteration number. Since the variance corresponds to the sum of the squares of the relative deviations of the calculated frequencies, it can possess values which represent the closeness of fit without regard to the signs of the absolute deviations. If the frequency parameters are replaced by the following substitutions

$$W_n = (1/\upsilon_n^o)^2 \qquad (29)$$

and

$$\Delta \upsilon_n^i = \upsilon_n^{i+1} - \upsilon_n^i \tag{30}$$

then Equation (28) can be rewritten in the form

$$\mathrm{Var}(i) = \sum_{n=1}^{s} W_n(\upsilon_n^i + \Delta \upsilon_n^i - \upsilon_n^o)^2 \tag{31}$$

or in matrix language as

$$\mathrm{Var}(i) = (\upsilon^i + \Delta\upsilon^i - \upsilon^o)^T W(\upsilon^i + \Delta\upsilon^i - \upsilon^o) \tag{32}$$

where W is a diagonal matrix, having elements $(W)_{nn} = (1/\upsilon_n^o)^2$ while the other matrices are sums of the component nxl column vectors.

The next step is to relate the changes in frequency, $\Delta\upsilon^i$, with the corresponding changes in the force constants, Δf^i . This is accomplished by using the Jacobian relationship

$$\Delta\upsilon^i = J_i(\Delta f^i) \tag{33}$$

where J_i is the i th Jacobian matrix having as elements

$$(J_i)_{nm} = \partial \upsilon_n^i / \partial f_m^i \tag{34}$$

where n = number of fundamentals while m = number of force constants. Using this relationship and substituting it for $\Delta\upsilon^i$ in Equation (32), the relationship of the variance to the corresponding changes in the force constants can be expressed in matrix form as

$$\begin{aligned}\mathrm{Var}(i) = {} & (\upsilon^i - \upsilon^o)^T W(\upsilon^i - \upsilon^o) + (\upsilon^i - \upsilon^o)^T W J_i \Delta f^i + \\ & (J_i \Delta f^i)^T W(\upsilon^i - \upsilon^o) + (J_i \Delta f^i)^T W J_i \Delta f^i\end{aligned} \tag{35}$$

Upon differentiation, the resulting expression is

$$\partial Var(i)/\partial(\Delta f^i) = (\upsilon^i - \upsilon^o)^T W J_i + (J_i \Delta f^i)^T W J_i \qquad (36)$$

from which, upon minimizing the variance (degree of fit) by setting

$$\partial Var(i)/\partial(\Delta f^i) = 0 \qquad (37)$$

and transposing terms, it follows that

$$\Delta f^i = (J_i^T W J_i)^{-1} J_i^T W (\upsilon^o - \upsilon^i) \qquad (38)$$

where Δf^i represents the force constant correction vector obtained from the i th iteration.

Equation (38) is used to refine the calculated frequencies υ_n^i. When the calculated frequencies approach values of the observed frequencies, υ_n^o, the elements of the Δf^i vector begin to vanish. Convergence then implies that the elements of the Δf^i vector have become so small that the frequency changes to which they would lead are negligible. To initiate the least squares refinement process, a trial set of force constants is chosen and an initial set of frequencies is computed. Then using Equation (38), a correction to the initial force constants is calculated and a new set of force constants computed from the relation

$$f_m^{i+1}(new) = f_m^i(old) + \Delta f_m^i \ . \qquad (39)$$

The process is repeated until $f_m^{i+1}(new) = f_m^i(old)$ or, in other words, until the correction vector vanishes. The final values of the force constants are then said to represent the "best set".

In the refinement Equation (38), most of the terms are

either known or can be computed to a high degree of accuracy. However, the Jacobian matrix elements, $\partial \upsilon_n^i / \partial f_m^i$, must be approximated. This drawback is the chief cause of several difficulties that may arise in the application of the refinement method. Mann et al. (71) in the first application of the force constant refinement procedure, computed the elements of the J_i matrix by giving small increments of 0.01 md./Å to each of the force constants and calculating the resultant frequencies. During their refinement process, however, they assumed the elements of the J_i matrix to remain constant. This type of approximation is valid only when the initially chosen set of force constants is not very different from the final refined set. In a different manner, Overend and Scherer (73,74) have applied first order perturbation theory and have approximated the elements of the J_i matrix during each iteration from appropriate linear combinations of the zeroth order eigenvectors of the symmetry factored (G'F')-matrix. This procedure of estimating the J_i matrix elements is quite often used although the inherent advantages are not obvious. In this investigation, a different Jacobian matrix was approximated during each iterative step of the force constant refinement procedure. An increment of 0.001 md./Å was given to a single force constant and the resultant vibration frequencies subsequently calculated. This process was repeated for each force constant and by this method, the ele-

ments of the i th Jacobian matrix, J_i, were computed row-wise. This approximation can be stated mathematically as

$$(J_i)_{nm} = \partial \upsilon_n^i / \partial f_m^i \cong \Delta \upsilon_n^i / \Delta f_m^i \qquad (40)$$

when here $\Delta f_m^i = 0.001$ md./Å.

It sometimes happens that the least squares refinement procedure does not produce converging values of the force constants. This can occur if the initial values chosen for the force constants are bad estimates thereby causing the correction vector, Δf^i, to contain some large elements with the overall result that these force constants are "overcorrected". Trouble of this sort, however, can be effectively cured by using only a fraction of the correction vector in the initial stages of the refinement process (75). With regard to this study, this fraction was 0.1-0.2 during initial iterations and near the convergence limit was chosen as 1.0 (full correction).

Nonconvergence will also occur if the matrix $(J_i^T W J_i)$ is nearly singular thereby causing large rounding errors when its inverse is taken in Equation (38) resulting in corresponding errors in the Δf_m^i vector. This situation, however, can be easily detected (76). A simple test for singularity is obtained by comparing the product of the diagonal elements with the determinant of a matrix. Both should be of a similar magnitude. If

$$\Pi_a (J_i^T W J_i)_{aa} \gg \left| J_i^T W J_i \right| \qquad (41)$$

then the matrix is close to being singular. Freeman and Henshall (77), using a damped least squares method, had overcome problems of singularity by adding to the $(J_i^T W J_i)$ matrix a scalar matrix B whose elements are defined as trace $(J_i^T W J_i)/M$ where M is a damping factor greater than unity. In this study, the damped least squares procedure with M = 10 was found to be advantageous in certain cases. Singularity, however, was not a major difficulty in this investigation. The various problems of nonconvergence, which are related to the least squares refinement of force constants, have been illustrated in graphic form by Bruton and Woodward (78).

One serious difficulty which arises in any force constant refinement procedure is the possibility that there are several distinct solutions to the force field which satisfactorily fit all the available data (79). The question of which minimum, if more than one, the calculation converges toward depends on the choice of initial force constants. Alternative solutions, if they exist, can only be found from force constant refinement calculations by systematically choosing a wide variety of initial force constants. In general, this is not practical. In relation to this investigation, all force constants obtained for the various dimeric M_2X_{10} transition metal pentahalides were found to be self consistent and therefore considered representative. The possibility of alternative solutions, however, was minimized but not completely eliminated.

The least squares refinement procedure itself is independent of the frequency assignment. Using a particular assignment and correctly matching the corresponding calculated and observed frequencies during each iteration, a "best set" of force constants along with a minimum variance (degree of fit) can be computed. The correct assignment, however, will produce the smallest possible minimum variance together with reasonable values of the force constants (72). In this way, the force constant refinement procedure can also serve as an aid in deducing the correct frequency assignment.

Diagonalization of (G'F')-matrix

Prior to any application of the force constant refinement process, it is first required to calculate vibrational frequencies from known force constants. To accomplish this task, it is necessary to solve the (G'F')-matrix for eigenvalues and eigenvectors (diagonalization). Both the G' and F' matrices are symmetric but oftentimes their product is not (60). It is not feasible to solve an unsymmetrical matrix for eigenvalues and eigenvectors using computer iteration methods. Several methods of overcoming this difficulty, however have been described elsewhere (80-83). One such commonly used diagonalization procedure (81) involves a transformation of the F' matrix. Such a diagonalization technique was employed in this study.

As was explained earlier, the symmetry factored character-

istic matrix equation for molecular vibration is written as

$$(G'F')L' = L'\Lambda \tag{42}$$

where Λ is the eigenvalue matrix containing the frequency parameters $4\pi^2 \upsilon_n^2$ on the main diagonal and L' is the transformation matrix from the normal coordinates to the internal symmetry coordinates. Since the G' matrix is symmetric, it can be diagonalized quite simply and its eigenvalue matrix, T, and eigenvector matrix, A, can be computed by standard methods (84). The characteristic equation of the G' matrix is represented as

$$G'A = AT \ . \tag{43}$$

A transformation matrix Z is then defined as

$$Z = AT^{\frac{1}{2}} \tag{44}$$

where $T^{\frac{1}{2}} = \text{diag}(t_1^{\frac{1}{2}}, t_2^{\frac{1}{2}}\text{---})$. The Z matrix can then be used to perform a transformation on the F' matrix. This transformation is symbolized in matrix form as

$$Z^T F'Z = H \tag{45}$$

where the matrix H is symmetric since A is orthogonal and T is diagonal while F' is symmetric. Consequently, if H is then diagonalized or, in other words, if the secular equation

$$HC = CE \tag{46}$$

is solved for both eigenvalues, E, and eigenvectors, C, it can be shown that the resultant eigenvalues are eigenvalues of the (G'F')-matrix or

$$E = \Lambda \tag{47}$$

and the eigenvectors of the (G'F')-matrix can be calculated from the relationship

$$L' = ZC \tag{48}$$

where C is the eigenvector matrix of the symmetric H matrix. These simplifications become obvious if the G' matrix is first expressed in terms of the Z matrix.

$$G' = ZZ^T \tag{49}$$

If Equation (45) is subsequently left multiplied on both sides by Z, there results the following series of matrix expressions:

$$ZZ^TF'Z = ZH \tag{50}$$

$$G'F'Z = ZH \tag{51}$$

$$Z^{-1}G'F'Z = H \tag{52}$$

Substitution of the last expression for H in the secular Equation (46) produces a new characteristic equation

$$(Z'G'F'Z)C = CE \tag{53}$$

$$\text{or} \quad (G'F')(ZC) = (ZC)E \tag{54}$$

Comparing Equation (54) with the characteristic matrix expression of molecular vibration represented by Equation (42), it is observed that

$$E = \Lambda \tag{55}$$

$$\text{and} \quad L' = ZC \tag{56}$$

and thus the unsymmetrical (G'F')-matrix is solved for both eigenvalues, Λ, and eigenvectors, L', by straightforward diagonalization of two symmetric matrices.

Data processing

In order to facilitate the various calculations involved in the force constant refinement procedure, two computer programs were developed with the aid of the Ames Laboratory Computer Services Group, Iowa State University of Science and Technology, Ames, Iowa. All computations were executed in Fortran IV G language on an IBM 360/65 computer.

One program, called GPROG, was specifically designed to compute the elements of the symmetry factored G' matrix of an M_2X_{10} system of D_{2h} symmetry. Input data for GPROG consisted of the eight molecular parameters of each dimeric transition metal pentahalide. A second, more general program, called FPROG was used for the force constant refinement process. Input parameters for FPROG contained the G' matrix elements, an assignment of the observed frequencies, a set of trial force constants and the number of desired iterations. The output data, computed after each iterative step, consisted of the following:

(a) calculated frequencies, υ_n^i

(b) refined force constants, f_m^i

(c) standard errors of force constants, σ_m^i

(d) correction vector, Δf_m^i

(e) variance, Var(i)

(f) average % frequency error, $\varepsilon(i)$

(g) potential energy distribution.

After each iteration of the FPROG program, the standard errors of the force constants, caused by the deviation of the calculated frequencies from the observed ones, were calculated by the statistical method of Ogawa and Miyazawa (61). A potential energy distribution of the internal symmetry coordinates in the normal coordinates (see Appendix F) was computed during each iteration to insure the correct alignment of calculated and observed frequencies for a particular assignment. After final refinement, the L' eigenvector matrix was calculated and printed out. Subroutine programs were employed for the matrix operations of multiplication, transposition and diagonalization. A subprogram in high speed disk mode was used for matrix inversion. To insure the validity of the various computer programs, trial calculations were first carried out on the CH_3Cl molecule with the result that the refined force constants and calculated fundamental frequencies closely paralleled the published values (57).

A graphic illustration of the force constant refinement process for the case of W_2Br_{10} is presented in Fig. 10. It can be seen that the variance, Var(i), is minimized completely after eighteen iterations. Initially, the trial force constants produced an average frequency deviation of 3.685% for the W_2Br_{10} molecule while the final refined values of the force constants minimized this deviation to 2.008%. The force constants computed after the eighteenth iteration were then termed the "best set" available.

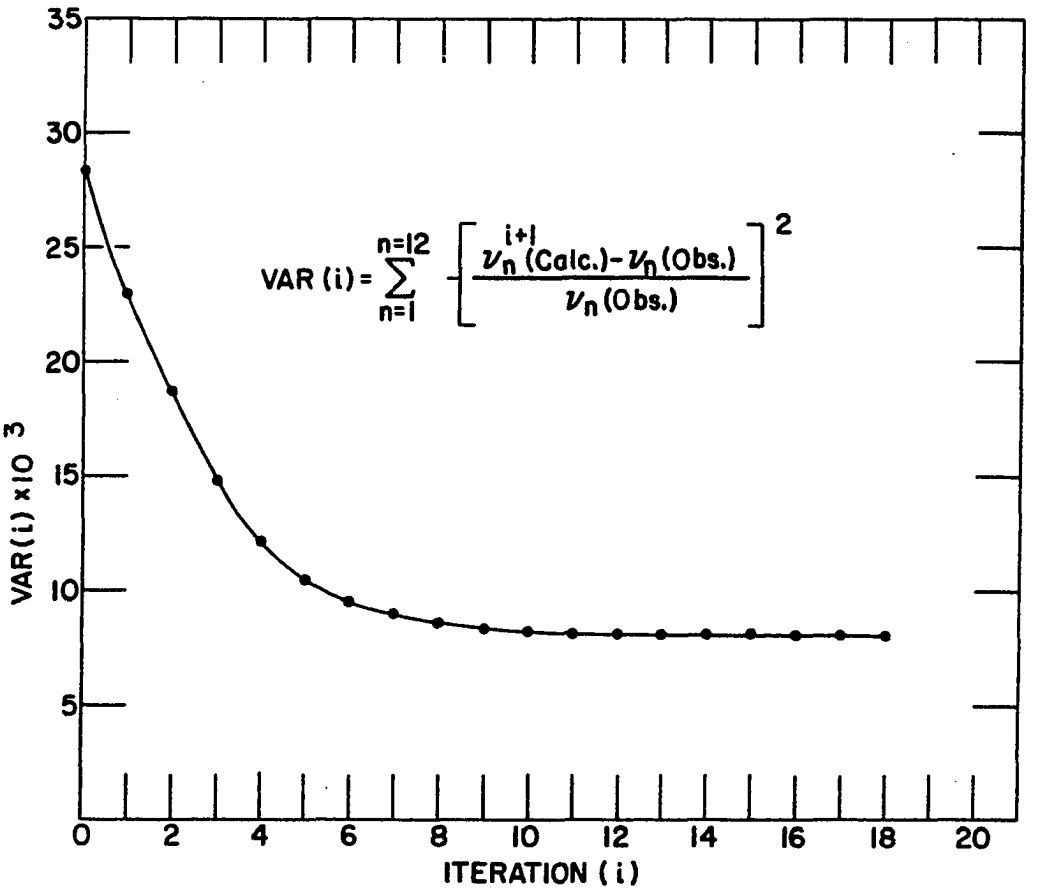

Fig. 10. Var(i) vs. i for W_2Br_{10}

The minimum obtainable variance depends in a critical way upon the particular choice of frequency assignment. Smallest values of the minimum variance are obtained for the correct frequency assignment (72). This specific property of the variance was found to be invaluable in the earlier stages of this study where a number of possible frequency assignments seemed applicable to the dimeric M_2X_{10} transition metal pentahalides.

Frequency Assignments of M_2X_{10}

Prior to the calculation of meaningful force constants, it is necessary to adopt a correct assignment for the vibrational frequencies. In this investigation, it was possible to assign the infrared spectra of the dimeric transition metal pentahalides: Nb_2X_{10} (X = Cl, Br), Ta_2X_{10} (X = Cl, Br, I), Mo_2Cl_{10}, W_2X_{10} (X = Cl, Br) and Re_2Cl_{10}. In the specific case of Nb_2I_{10}, because of large vibrational coupling effects and possible breakdown of the force field, the least squares adjustment process did not refine the initially chosen force constants nor minimize the frequency differences to acceptable values. Niobium(V) iodide does, however, represent an extreme case since the iodine atoms are considerably more massive than the niobium atoms and large mode coupling effects are to be expected. For the other cases of dimeric M_2X_{10} transition metal pentahalides, there are basically three sets

of infrared active fundamentals. One group is concerned primarily with the four infrared active terminal metal-halogen stretches. A second set contains the two bridged metal-halogen stretches while a final set is comprised of the seven infrared allowed metal-halogen bending fundamentals.

Terminal metal-halogen stretches

The four highest frequency fundamentals, observed in the infrared absorption spectra of the dimeric transition metal pentahalides, were assigned to the four infrared allowed terminal M-X stretches predicted from D_{2h} symmetry. In a past study, Walton and Brisdon (42), from an infrared study of some M_2X_{10} metal halides, have also included the bridging fundamentals in this frequency region and thus postulated six high frequency absorption bands. Their argument was based on an accepted frequency difference of ca. 50 cm.$^{-1}$ between bridging and terminal ν(M-Cl) frequencies arrived at from a previous investigation (85) of some bridged halides of palladium and platinum. As was observed in this study, however, the frequency difference between the bridged and terminal metal-halogen stretches is dependent upon both the central metal atom and the corresponding halogen atom. In the infrared spectra of all of the M_2X_{10} pentahalides investigated in this work, only four high frequency fundamentals were observed in each case.

The terminal metal-halogen stretching fundamentals were

assigned on the basis of previous infrared studies of similar fundamentals (50,86) and on the basis of generally accepted vibrational considerations regarding the relative energies of various modes (49,87). The assignments of the infrared active terminal M-X stretching fundamentals were arranged according to their vibrational energies as

$$\nu_1(B_{1u}) > \nu_{10}(B_{3u}) > \nu_5(B_{2u}) > \nu_6(B_{2u}) \qquad (57)$$

where a schematic description of the modes was seen in Fig. 7. It is noted that the four bands comprise three different symmetry types thus maintaining resonance interaction at a minimum. Such an explanation can account for the close arrangement of the high frequency bands in the spectra of the dimeric pentahalides. This particular assignment of the terminal M-X stretches is equivalent to that chosen by Werder et al. (33) for the case of Nb_2Cl_{10}, although it is different from that recently employed by Beattie et al. (88) whose infrared assignments of the M_2X_{10} halides (M = Nb, Ta; X = Cl, Br) are considered somewhat dubious in light of the results of this study. In the assignment chosen for this investigation, the relative ordering of the ν_{10} and ν_5 modes is compatible with the ordering of similar vibrational modes in the infrared spectra of the previously studied planar-bridged M_2X_6 metal halogen systems (64,65).

El-Sayed and Kaesz (89) had obtained the infrared spectra of systems which are comparable to the M_2X_{10} pentahalides.

They interpreted the infrared spectra, in the carbonyl region, of the compounds $M(CO)_4X$ (M = Mn, Tc, Re; X = Cl, Br, I) on the basis of a dimeric D_{2h} structure possessing bridging halogens. Their choice of assignment of the four infrared active C≡O stretching modes in the $M_2X_2(bridge)(CO)_8$ system was entirely vibrationally consistent with that assignment of the terminal M-X stretches employed in this investigation. The metal(V) halides can be similarly formulated as $M_2X_2(bridge)X_8$. Such a comparison of two totally different vibration types provides an example of a case whereby a high frequency assignment, such as carbonyl stretching modes, can be useful in establishing the character of lower frequency modes, such as metal-halogen stretches.

Bridged metal-halogen stretches

The two band maxima observed at intermediate frequencies in the infrared spectra of the dimeric transition metal pentahalides were assigned to the two infrared allowed bridged M-X stretching modes, ν_7 and ν_{11}, predicted from D_{2h} symmetry. According to this particular assignment, $\nu_7(B_{2u})$ was considered to be at higher energies than $\nu_{11}(B_{3u})$ for all of the pentahalides studied except Ta_2I_{10} where, because of geometrical considerations, the reverse arrangement was held to be valid. The assignment of the bridged metal-halogen stretching modes in M_2X_{10} was consistent with that employed by previous workers (33,88).

In Table 9, spectral data are presented for the infrared active bridged metal-chlorine stretching vibrations of several symmetric doubly halogen bridged metal chlorides. It can be seen that the vibrational frequencies associated with the bridged M-Cl stretching modes are a critical function of such factors as the nature of the metal atom and its related mass and coordination number.

Table 9. Some bridged metal-chlorine stretching frequencies in the infrared

Species	Metal atom coordination[a]	ν(M-Cl$_B$) cm.$^{-1}$		Ref.
$Cu_2Cl_6^{2-}$	square planar	278	236	(90)
$Pd_2Cl_6^{2-}$	"	305	263	(64)
$Pt_2Cl_6^{2-}$	"	315	302	(64)
Au_2Cl_6	"	310	305	(65)
Al_2Cl_6	tetrahedral	420	(338)[b]	(62)
Ga_2Cl_6	"	305	287	(63)
Nb_2Cl_{10}	octahedral	251	223	this work
Mo_2Cl_{10}	"	276	238	"
Ta_2Cl_{10}	"	251	225	"
W_2Cl_{10}	"	283	247	"
Re_2Cl_{10}	"	276	255	"

[a]Approximate coordination.

[b]Calculated value.

Metal-halogen bends

The majority of the band maxima observed in the metal-halogen bending region of the infrared were assigned primarily on the basis of the results of previous vibrational studies of metal halides containing similar vibrational modes (64,91,92). As stated previously, the M-X bending mode of M_2X_{10} represented as $\upsilon_4(B_{1u})$ is a low frequency ring deformation mode and was not observed down to 42.5 cm.$^{-1}$ (instrument limit). Some difficulties ensued when three metal-halogen bending modes could not be initially assigned because of their apparent similarity. In that event, the particular assignment which best reproduced the observed frequencies was chosen to be the correct one. For the case of Nb_2Cl_{10}, six trial assignments were used in the force constant refinement procedure but only one such assignment produced a reasonable set of force constants and an extremely small value of the minimum variance (degree of fit). That particular assignment was chosen for further calculations and was subsequently found to be self consistent with respect to the infrared spectra of all of the dimeric transition metal pentahalides investigated.

Frequency relationships

The various assignments of the infrared spectra of the dimeric transition metal pentahalides are contained in Tables 10 and 11. It is of interest to note the various shifts in those frequencies associated with the metal-halogen stretching

Table 10. Assignment of M_2Cl_{10} observed infrared frequencies ($cm.^{-1}$)

	Assignment	Nb_2Cl_{10}	Mo_2Cl_{10}	Ta_2Cl_{10}	W_2Cl_{10}	Re_2Cl_{10}
B_{1u}	(ν_1) Asymm. M-X(axial) stretch	423	412	411	398	404
	(ν_2) Out of plane M-X_2 wag	171	172	164	166	168
	(ν_3) Out of plane M-X_4 wag	116	117	119	121	118
	(ν_4) Ring deformation	0.0[a]	0.0[a]	0.0[a]	0.0[a]	0.0[a]
B_{2u}	(ν_5) Symm. M-X(equat.) stretch	400	380	385	365	369
	(ν_6) Symm. M-X(axial) stretch	365	347	364	334	350
	(ν_7) Asymm M-X(bridge) stretch	251	276	251	283	276
	(ν_8) In plane M-X_2(equat.) bend	197	214	200	203	216
	(ν_9) M-X_2(axial) bend	154	159	148	148	157
B_{3u}	(ν_{10}) Asymm. M-X(equat.) stretch	412	391	402	379	393
	(ν_{11}) Symm. M-X(bridge) stretch	223	238	225	247	255
	(ν_{12}) M-X_2(axial) bend	142	143	138	141	148
	(ν_{13}) In plane MX_2 rock	73	75	71	72	83

[a]No iteration.

Table 11. Assignment of M_2X_{10} observed infrared frequencies ($cm.^{-1}$)

	Assignment	Nb_2Br_{10}	Ta_2Br_{10}	W_2Br_{10}	Ta_2I_{10}
B_{1u}	(ν_1) Asymm. M-X(axial) stretch	299	261	260	197
	(ν_2) Out of plane M-X_2 wag	112	112	114	83
	(ν_3) Out of plane M-X_4 wag	77	79	73	61
	(ν_4) Ring deformation	0.0[a]	0.0[a]	0.0[a]	0.0[a]
B_{2u}	(ν_5) Symm. M-X(equat.) stretch	263	244	244	176
	(ν_6) Symm. M-X(axial) stretch	219	217	212	155
	(ν_7) Asymm. M-X(bridge) stretch	159	162	179	107
	(ν_8) In plane M-X_2(equat.) bend	127	127	129	95
	(ν_9) M-X_2(axial) bend	105	102	103	77
B_{3u}	(ν_{10}) Asymm. M-X(equat.) stretch	283	251	253	186
	(ν_{11}) Symm. M-X(bridge) stretch	145	147	158	116
	(ν_{12}) M-X_2(axial) bend	96	96	95	73
	(ν_{13}) In plane MX_2 rock	63	63	63	45

[a]No iteration.

vibrations. Since it is the metal-halogen stretching modes which can relate useful information concerning the strengths of the various metal-halogen bonds, they comprised the fundamental modes of prime interest in this investigation.

The shifts to lower frequencies of the terminal M-X stretches on going from Cl to Br to I, while keeping the central metal atom unchanged, are those which would ordinarily be expected for metal halides. It was also observed that on proceeding to the heavier pentahalides of the same transition metal, the frequencies associated with the bridged M-X stretches begin to increasingly rank in energy with those frequencies corresponding to the terminal M-X stretching modes. Such a trend would seem to indicate the increasing stability of the M-X (bridge) bond relative to the M-X (terminal) bond on going from chloride to bromide to iodide. Similar frequency trends have been observed by Adams *et al.* (64) in the infrared spectra of the planar symmetrically di-bridged anionic halides of platinum(II), $[Pt_2X_6]^{2-}$ (X = Cl, Br, I).

As the halogen atom remained unchanged while the central transition metal atom of the dimeric pentahalide was varied within a Group, accompanying changes occurred in the position of the metal-halogen stretching frequencies. In the infrared spectra of the pentachlorides and pentabromides of niobium and tantalum, the frequencies associated with the terminal metal-halogen stretches decreased on going from the niobium penta-

halide to the tantalum pentahalide, while on the other hand, the corresponding bridged metal-halogen stretching frequencies remained approximately constant. Similar frequency shifts were seen to occur in the infrared spectra of the pentachlorides of the Group VIB heavy transition metals, with the minor difference that the bridged metal-chlorine stretching frequencies increased slightly on going from Mo_2Cl_{10} to W_2Cl_{10}. Prior to any force constant calculation, it was difficult to assess such frequency shifts as these that occur within a Group since the mass changes on proceeding to heavier metals in the same Group exert considerable influence on the positions of the M-X stretching frequencies.

It is usually more convenient to analyze the frequency changes in the infrared spectra of the corresponding pentahalides of the transition metals of the same period since any frequency shifts due to mass effects are minimized. In relation to the infrared spectra of the second series pentachlorides, it was observed that the terminal M-Cl stretching frequencies of Mo_2Cl_{10} occurred at lower values than those observed for Nb_2Cl_{10} while the reverse arrangement applied to the bridged M-Cl stretching frequencies. This would seem to indicate the increasing energy of the vibrational modes associated with the stretching of the M-Cl (bridge) bonds on proceeding from niobium (d^0) to molybdenum (d^1) pentachloride. Analogous frequency shifts were observed in the infrared

spectra of the pentachlorides and pentabromides of the third series transition metals tantalum and tungsten. The infrared spectrum of the dimeric rhenium(V) chloride, however, did not smoothly fit into this trend. The terminal M-Cl stretching frequencies of Re_2Cl_{10} attained values smaller than those of Ta_2Cl_{10} but slightly larger than those corresponding to W_2Cl_{10}. On the other hand, the frequencies associated with the bridged M-Cl stretching modes of Re_2Cl_{10} were comparable to those of W_2Cl_{10}, where the bridged M-Cl stretching vibrations occurred at significantly higher vibrational energies than the corresponding vibrational modes of Ta_2Cl_{10}.

In light of these results, it can generally be stated for the case of the heavier transition metal halides that, on going from the heavy metals of Group VB to those of Group VIB or Group VIIB, the bridged metal-halogen stretching modes become increasingly energetic relative to the terminal metal-halogen stretching vibrations. It would be indeed risky to extend such an argument to include the entire transition metal series; nevertheless, there are some points of interest. In the infrared spectra of the chlorides of the heavy metals at the end of the transition series, the average difference between the terminal M-Cl stretches and bridged M-Cl stretches is reported as ca. 50 $cm.^{-1}$ for the cases of the planar species $[M_2Cl_6]^{2-}$ (M = Pd, Pt) (64) and Au_2Cl_6 (65, 88). From the present investigation, it was concluded that the corresponding

difference between terminal and bridged M-Cl stretching frequencies is ca. 100 $cm.^{-1}$ in the cases of the dimeric pentachlorides of heavy metals occurring early in the transition series. A comparison of such frequency differences would therefore indicate that halogen-bridge bonding plays a more important role in the halides of the metals at the end of the transition series.

Force Constants of M_2X_{10}

From the far infrared absorption spectra of the dimeric transition metal pentahalides, M_2X_{10}, it was possible to calculate nine vibrational force constants. Descriptions of the various force constants are presented in Table 12.

Table 12. Description of M_2X_{10} force constants

Force constant	Description
f_S	axial M-X stretching
f_T	equatorial M-X stretching
f_R	bridged M-X stretching
f'_{SS}	MX(axial)-MX(axial) str. interaction
f_α	X(equatorial)-M-X(equatorial) bend
f_V	X(equatorial-M-X(axial) bend
f_u	X(axial)-M-X(bridge) bend
f_γ	X(equatorial-M-X(bridge) bend
$f_{R\gamma}$	M-X(bridge) str.-bend interaction

It was necessary to include an opposite bond stretch interaction constant, f'_{ss}, in order to fit the infrared spectra of the majority of the M_2X_{10} halides. Such an interaction constant was expected to be significant in cases where the halogen atom was massive in comparison to the metal atom. In a similar manner, $f_{R\gamma}$, the only off-diagonal force constant employed, attained significant values in cases where light metal atoms were bonded to heavy halogen atoms.

The values of the force constants of several M_2X_{10} heavy metal halides are presented in Tables 13 and 14 along with the corresponding standard deviations caused by the differences between the observed and calculated frequencies. Each standard error term was a function of all of the frequency residues. It was observed, however, that the standard deviations of the force constants generally increased as the degree of frequency fit decreased. The observed and calculated infrared frequencies are contained in Appendix G.

There were two types of terminal M-X bond force constants computed from the infrared spectra of the M_2X_{10} halides. One, labelled as f_S, involved the stretching of the M-X (axial) bonds while the other was associated with the stretching of the M-X (equatorial) bonds and was symbolized as f_T. It can be seen from Tables 13 and 14 that $f_S \cong f_T$ when $f'_{ss} \cong 0$. This is the expected result since f_S does not principally determine the positions of the associated M-X (axial) stretching vibra-

Table 13. Force constants of some dimeric heavy metal pentachlorides

Force constant mdyne. (Å)$^{-1}$	Nb_2Cl_{10}	Mo_2Cl_{10}	Ta_2Cl_{10}	W_2Cl_{10}	Re_2Cl_{10}
f_s	2.395±0.005	2.26 ±0.02	2.68 ±0.03	2.32 ±0.01	2.478±0.005
f_T	2.20 ±0.02	1.97 ±0.06	2.63 ±0.03	2.25 ±0.05	2.40 ±0.06
f_R	0.84 ±0.09	1.17 ±0.02	0.88 ±0.02	1.25 ±0.01	1.17 ±0.01
f'_{ss}	0.416±0.005	0.26 ±0.02	0.08 ±0.03	0.01 ±0.01	0.070±0.005
f_α	0.29 ±0.02	0.345±0.007	0.311±0.007	0.313±0.002	0.349±0.003
f_v	0.174±0.005	0.170±0.003	0.155±0.002	0.150±0.003	0.163±0.003
f_u	0.156±0.005	0.165±0.004	0.189±0.003	0.202±0.005	0.204±0.005
f_γ	0.12 ±0.01	0.103±0.002	0.110±0.006	0.096±0.001	0.145±0.001
$f_{R\gamma}$	0.01 ±0.02	0.05 ±0.01	0.002±0.016	0.034±0.005	0.004±0.002
Ave. freq. dev. (%) =	1.714	1.721	1.417	1.159	1.253
Var(min.)x10^2 =	0.5718	0.5567	0.4354	0.3048	0.4142

Table 14. Force constants of some dimeric heavy metal pentahalides

Force constant mdyne. (Å)$^{-1}$	Nb_2Br_{10}	Ta_2Br_{10}	W_2Br_{10}	Ta_2I_{10}
f_s	1.76 ±0.02	1.888±0.006	1.835±0.006	1.31 ±0.02
f_T	1.31 ±0.08	1.63 ±0.02	1.61 ±0.07	0.83 ±0.20
f_R	0.74 ±0.07	0.83 ±0.01	1.14 ±0.05	1.00 ±0.07
f'_{ss}	0.52 ±0.02	0.355±0.005	0.291±0.006	0.32 ±0.02
f_α	0.16 ±0.02	0.177±0.007	0.211±0.007	0.22 ±0.07
f_v	0.176±0.009	0.169±0.006	0.173±0.006	0.142±0.005
f_u	0.142±0.006	0.160±0.005	0.141±0.004	0.154±0.005
f_γ	0.22 ±0.02	0.205±0.003	0.171±0.006	0.126±0.005
$f_{R\gamma}$	0.08 ±0.02	0.074±0.004	0.09 ±0.02	0.10 ±0.06
Ave. freq. dev. (%) =	3.064	1.411	2.008	2.665
Var(min.)x10^2 =	2.0394	0.4692	0.8078	2.2265

tions. As illustrated in the factored F' matrix in Fig. 9, the M-X (axial) stretching vibrations are determined primarily from linear combinations of the force constants $f_s \pm f'_{ss}$. The M-X (equatorial) stretching vibrations are, however, principally related to a single bond force constant, f_T. For these reasons, the more independent force constant f_T was chosen to represent the terminal M-X bond force constant.

The bending force constants of the dimeric M_2X_{10} metal pentahalides were ca. 1/10 the values of the bond stretching force constants as is usually the case among most molecules (60). Values of the bending force constants were observed to remain approximately constant and did not appear to be particularly dependent upon either the metal or the halogen atom. On the other hand, however, the bond force constants did appear to be critical functions of both the metal and halogen atoms. The terminal M-X bond force constants of the pentahalides of a particular metal were related in the usual manner as $f_T(M\text{-}I) \cong 0.7f_T(M\text{-}Br) \cong (0.7)^2 f_T(M\text{-}Cl)$. In a similar halogen series, however, the bridged M-X force constants, f_R, did not appear to be distinctly dependent upon the halogen atom. Values of the f_R/f_T ratio increased on going to the heavier pentahalides of the same transition metal. These results are contained in Table 15. The pentahalides of tantalum provided a complete series for comparison. The calculated bond force constants of the Ta_2X_{10} compounds indicated a definite dependence upon the

Table 15. Values of f_R/f_T for M_2X_{10}

Compound	f_R/f_T
Nb_2Cl_{10}	0.380 ± 0.043
Nb_2Br_{10}	0.563 ± 0.097
Ta_2Cl_{10}	0.335 ± 0.012
Ta_2Br_{10}	0.511 ± 0.014
Ta_2I_{10}	1.212 ± 0.370
Mo_2Cl_{10}	0.519 ± 0.029
W_2Cl_{10}	0.556 ± 0.014
W_2Br_{10}	0.708 ± 0.064
Re_2Cl_{10}	0.485 ± 0.016

halogen atom.

$$f_T(Ta_2Cl_{10}) \cong 3f_R(Ta_2Cl_{10}) \quad (58)$$

$$f_T(Ta_2Br_{10}) \cong 2f_R(Ta_2Br_{10}) \quad (59)$$

$$f_T(Ta_2I_{10}) \cong f_R\ (Ta_2I_{10}) \quad (60)$$

A similar relationship was observed for the pentachloride and pentabromide of niobium.

$$f_T(Nb_2Cl_{10}) \cong 3f_R(Nb_2Cl_{10}) \quad (61)$$

$$f_T(Nb_2Br_{10}) \cong 2f_R(Nb_2Br_{10}) \quad (62)$$

Strictly speaking, bond dissociation energies, V_d, are not proportional to bond force constants, $f_R = (\partial^2 V/\partial R^2)_0$ (93). As a crude first approximation, however, they can be considered so. With this in mind then, a comparison of the bond

force constants for the pentahalides of niobium and tantalum indicated that halogen bridge bonding becomes increasingly favorable as the size of the halogen atom increases. This was also found to be true for the tungsten(V) halides. Similar trends have also been documented by Adams et al. (64) for the cases of the dimeric halide anions of Pd(II) and Pt(II). It appears then, at first sight, that halogen bridge bonding becomes energetically favorable in the order I > Br > Cl for the heavy transition metal halides.

In order to evaluate the effects of the nature of the metal atom on the bond force constants, the dimeric heavy transition metal pentachlorides, M_2Cl_{10}, were studied in further detail. The dimeric pentachlorides provide an appropriate series for purposes of comparison since interaction effects are minimized because of the lighter mass of the Cl atom relative to the heavy metal atom. Furthermore, exact structural data are available for the solid dimeric pentachlorides (24,25,27,29). For the M_2Cl_{10} compounds, the values of the terminal M-Cl stretching force constant, f_T, and the bridged M-Cl stretching force constant, f_R, are illustrated graphically in Fig. 11. Here it can be seen that on going from the Group VB heavy metals to those of Groups VIB and VIIB, the binding strength of the M-Cl bridge bond has increased in relation to that of the terminal M-Cl bond. The apparent anomaly of the dimeric Re_2Cl_{10} is not easily understood in

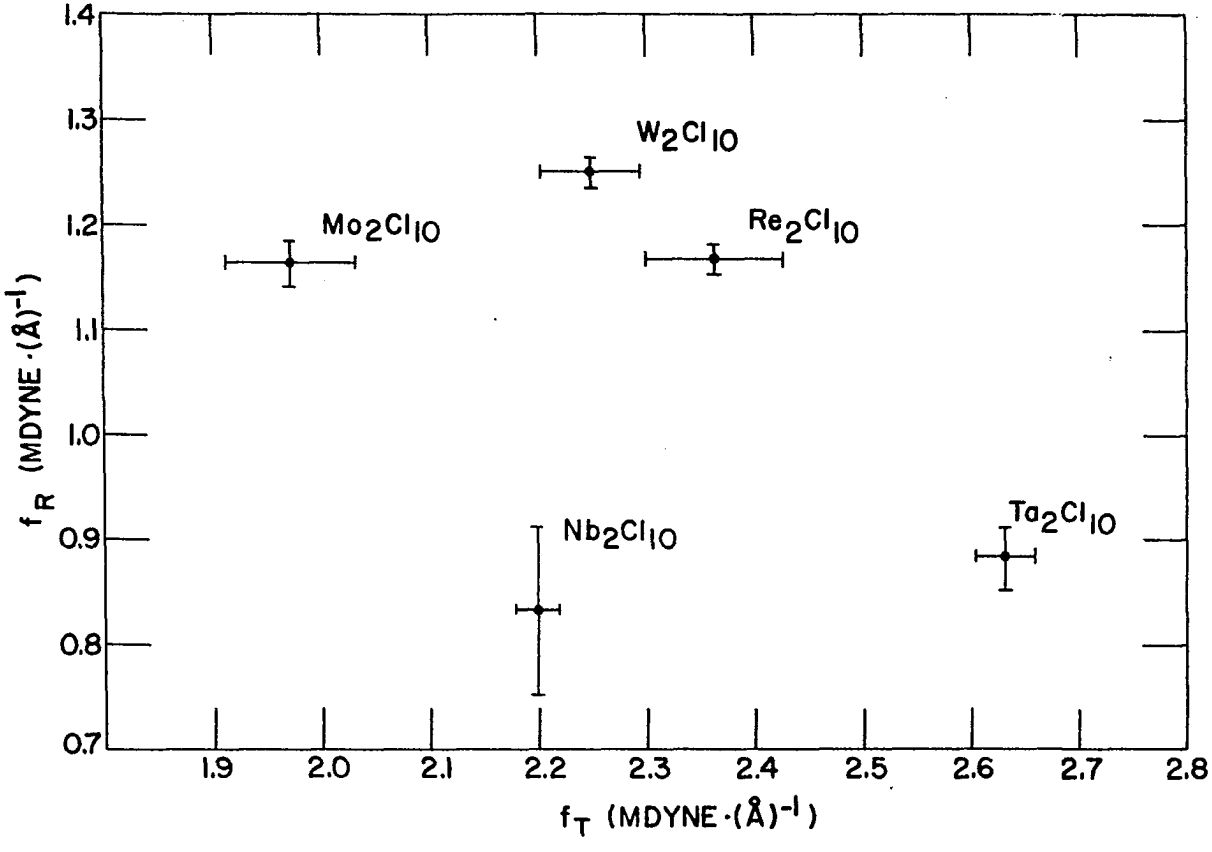

Fig. 11. f_R vs. f_T for M_2Cl_{10} (M = Nb, Ta, Mo, W, Re)

the absence of any thermodynamic data (94). From the general trend of force constants, however, halogen bridge bonding would appear to play a more important role in the Group VIB and VIIB heavy metal pentahalides than in the pentahalides of the Group VB metals. In an analogous manner, it can be deduced that bridged metal-halide bonds relative to terminal metal-halide bonds appear to be favored more in the pentahalides of the lighter metals (Nb, Mo) of Groups VB and VIB than in the pentahalides of the corresponding heavier metals (Ta, W) of the same groups.

Several experimental results by previous workers are in general agreement with these conclusions. As in the case of the terminal M-X stretching force constants of the M_2Cl_{10} compounds, the terminal bond stretching force constants for the metal hexafluorides are also higher for the third row transition elements than for the corresponding second row elements and decrease within each series (1). Both niobium and tantalum pentachloride exist as monomers in the gas phase (17,18) while there is a report (15) which claims that tungsten(V) chloride may exist in appreciable concentrations as W_2Cl_{10} dimers in the vapor state. Such results indicate the greater preference of halogen bridge bonding in the Group VIB heavy metal pentahalides.

It is of some interest to extend the results of the transition metal pentahalides to the lower valent halides of the

2nd and 3rd row transition metals of Groups VB and VIB. The general stabilities of these lower valent halides are in accord with the data of this investigation. The majority of metal halides, containing the M_6X_{12} cluster units (M = Nb, Ta), possess one type of halogen atom which bridges two metal atoms (95). On the other hand, the majority of compounds containing the M_6X_8 clusters (M = Mo, W) each have one type of halogen atom bridging three metal atoms (96). These results demonstrate the greater favorability of halogen bridge bonding in the cases of the lower halides of the Group VIB metals as compared to the Group VB heavy metal halides.

A compound containing the Nb_6I_8 metal halide cluster has been shown to exist in the solid state (97) while compounds containing the corresponding Nb_6Cl_8 and Nb_6Br_8 clusters have not been reported. These results would seem to follow the trend of increasing M-X (bridge) bond stability with increasing size of the halogen atom.

Lower valent metal halides containing the Nb_6F_{12} (98) and Nb_6I_8 (97) clusters are stable solids at room temperature while the corresponding halides containing the Ta_6F_{12} or Ta_6I_8 metal halide cluster units are not known at the present time. Such a crude comparison would appear to confirm the greater stability of the M-X bridge bond in the halides of the lighter metal (Nb) of Group VB relative to the halides of the heavier tantalum.

While the apparent stabilities of a number of lower valent heavy transition metal halides are consistent with the results of this investigation, it would be indeed risky to extend the force constant relations too far. A myriad of other factors such as oxidation state, electronic structure, thermodynamic and kinetic stability exert considerable influence on the physical properties of metal halides. In this study, however, using some very simple force constant analyses of some higher halides of transition metals, some insight into the nature of the lower valent transition metal halides can be attained.

Potential Energy Distributions

The potential energy associated with a particular fundamental vibration is comprised of the potential energies of the component symmetry coordinates. The character of the normal vibrational frequency is principally determined by that symmetry coordinate which contributes the largest share of the potential energy (99). It sometimes happens, however, that two or more symmetry coordinates possess similar shares in the potential energy distribution. In that event, the character of the vibrational frequency is determined by several symmetry coordinates. Since a symmetry coordinate is associated with a particular type of internal coordinate, the internal coordinate character (stretch, bend, etc.) of a fundamental vibrational frequency can be established from a potential energy distribu-

tion.

From the final refined sets of force constants for the M_2X_{10} metal halides, final L' eigenvector matrices were computed. A knowledge of the L' matrix made it possible to calculate a distribution of potential energies of the symmetry coordinates in that normal coordinate associated with a particular normal vibrational frequency (see Appendix F). Relative potential energy distributions of the symmetry coordinates in the normal coordinates are contained in Appendix H for the infrared allowed fundamental vibrations of the dimeric M_2X_{10} heavy transition metal pentahalides. From this type of study, it was observed that the character of the metal-halogen fundamental vibrations became increasingly complex on proceeding to the heavier halides of a particular metal. For example, the 259 cm.$^{-1}$ band in Nb_2Cl_{10} was associated primarily with a bridged Nb-Cl stretching mode (υ_7) while the corresponding 152 cm.$^{-1}$ band in Nb_2Br_{10} was principally associated with both a bridged Nb-Br stretching mode (υ_7) and a terminal Nb-Br stretching mode (υ_5). Conversely, on going to the heavier metal halides, mode coupling diminished. This is demonstrated by comparing the potential energy distribution of the lightest metal chloride, Nb_2Cl_{10}, to that of the heaviest metal chloride, Re_2Cl_{10}, studied. The 200 cm.$^{-1}$ band in the infrared spectrum of Nb_2Cl_{10} has both M-Cl bending (υ_8) and bridged M-Cl stretching (υ_7) character. On the

other hand, the corresponding 215 cm.$^{-1}$ band of Re_2Cl_{10} was comprised of almost entirely M-Cl bending (υ_8) character. In the two extreme cases of Nb_2Br_{10} and Ta_2I_{10}, it was observed for a few frequencies that the largest terms in the potential energy distributions did not correspond to the particular assigned modes. This was a direct result of intense mode interaction and inadequacies in the potential field. In these instances, however, the second largest terms in the potential energy distributions were associated with the assigned modes. For the majority of bands reported for Nb_2Br_{10} and Ta_2I_{10}, however, the largest terms in the potential energy distributions did correspond to the assigned modes.

It was generally concluded that, as the halogen atoms became massive in comparison to the metal atoms, the degree of mode coupling increases, producing the overall result that makes it difficult to invoke distinct band assignments in the infrared spectra of the dimeric heavy transition metal pentahalides.

SUGGESTIONS FOR FUTURE WORK

This type of vibrational study can be extended to similar halogen bridged compounds containing the metal atom in a low formal oxidation state. Some monoadducts of several heavy transition metal tetrahalides, $MX_4 \cdot L$, may exist in a dimeric form possessing a metal-metal bond in addition to the metal-ligand bonds. Since the symmetry of such compounds would permit a large number of infrared active fundamentals, the related normal coordinate analyses would provide valuable information concerning the strength of the metal-metal bond in relation to the other types of bonds present in such compounds. Structural data, however, must be obtained prior to such vibrational analyses.

In order to investigate further the nature of halogen bridge bonding in metal halides, the vibrational spectra of a number of metal compounds containing differing systems of bridging halogens would be of value. Particularly with the recent advent of laser techniques, the low frequency Raman spectra of a number of heavy metal compounds can now be determined. With the possibility of obtaining both the low frequency Raman and infrared absorption spectra of the heavier transition metal halides, the corresponding normal coordinate analyses and force constant calculations can be carried out on the highly symmetrical metal halide complexes whose far infrared spectra exhibit a minimum of absorption bands.

BIBLIOGRAPHY

1. Gutmann, V. Halogen chemistry. Vol. 3. New York, New York, Academic Press, Inc. 1967.

2. Colton, R. and Tomkins, I. B., Austral. J. Chem. 18, 447 (1965).

3. Knox, K., Tyree, S. Y., Srivastova, R. D., Normon, V., Bassett, J. Y. and Holloway, J. H., J. Am. Chem. Soc. 79, 3358 (1957).

4. Brewer, L., Bromley, L. A., Gilles, P. W. and Lofgren, N. L. In Quill, L. L., ed. The chemistry and metallurgy of miscellaneous materials. Pp 76-192. New York, New York, McGraw-Hill Book Co., Inc. 1950.

5. Allen, E. A., Brisdon, B. J. and Fowles, G. W. A., J. Chem. Soc. 1964, 4531 (1964).

6. Novikov, G. I., Andreeva, N. V. and Polyachenok, O. G., Russ. J. Inorg. Chem. 6, 1019 (1961).

7. McCarley, R. E. and Brown, T. M., Inorg. Chem. 3, 1232 (1964).

8. Knox, K. and Coffey, C. E., J. Am. Chem. Soc. 81, 5 (1959).

9. Brown, D. and Colton, R., J. Chem. Soc. 1964, 714 (1964).

10. Geilmann, W. and Wrigge, F. W., Z. anorg. allgem. Chem. 214, 248 (1933).

11. Colton, R., J. Chem. Soc. 1962, 2078 (1962).

12. Alexander, K. M. and Fairbrother, F., J. Chem. Soc. 1949S, 223 (1949).

13. Alexander, K. M. and Fairbrother, F., J. Chem. Soc. 1949, 2472 (1949).

14. Shchukarev, S. A. and Novikov, G. I., J. Inorg. Chem. U.S.S.R. 1, No. 3: 6 (1956).

15. Shchukarev, S. A., Novikov, G. I., Vasil'Kova, I. V., Suvarov, A. V., Andreeva, N. V., Sharupin, B. N. and Baev, A. K., Russ. J. Inorg. Chem. 5, 802 (1960).

16. Shchukarev, S. A. and Kovonin, G. A., Russ. J. Inorg. Chem. 9, 715 (1964).

17. Balke, C. W. and Smith, E. F., J. Am. Chem. Soc. 30, 1637 (1908).

18. Schäfer, H. and Sibbing, E., Z. anorg. allgem. Chem. 305, 341 (1960).

19. Skinner, H. H. and Sutton, L. E., Trans. Faraday Soc. 36, 668 (1940).

20. Spiridonov, V. P. and Romanov, G. U., Vest. Mosk. Univ., Ser. II 21, 109 (1966). Original not available; abstracted in Chemical Abstracts 66: 89278e. 1966.

21. Ewens, R. V. G. and Lister, M. W., Trans. Faraday Soc. 34, 1358 (1938).

22. Spiridonov, V. P. and Romanov, G. U., Vest. Mosk. Univ., Ser. II 22, 98 (1967). Original not available; abstracted in Chemical Abstracts 67: 15868w. 1967.

23. Rinke, K. and Schäfer, H., Angew. Chem. 6, 637 (1967).

24. Zalkin, A. and Sands, D. E., Acta Cryst. 11, 615 (1958).

25. Sands, D. E. and Zalkin, A., Acta Cryst. 12, 723 (1959).

26. Colton, R. and Tomkins, I. B., Austral. J. Chem. 19, 759 (1966).

27. Boorman, P. M., Greenwood, N. N., Hildon, M. A. and Whitfield, H. J., J. Chem. Soc. 1967A, 2017 (1967).

28. Smith, G. S., Johnson, Q. and Elson, R. E., Acta Cryst. 22, 300 (1967).

29. Mucker, K., Smith, G. S. and Johnson, Q., Acta Cryst. 24B, 874 (1968).

30. Klemm, W. and Steinberg, H., Z. anorg. allgem. Chem. 227, 193 (1936).

31. Brisdon, B. J., Edwards, D. H., Machin, D. J., Murray, K. S. and Walton, R. A., J. Chem. Soc. 1967A, 1825 (1967).

32. Kepert, D. L. and Nyholm, R. S., J. Chem. Soc. 1965, 2871 (1965).

33. Werder, R. D., Frey, R. A. and Günthard, H. H., J. Chem. Phys. 47, 4159 (1967).

34. McCarley, R. E. and Torp, B. A., Inorg. Chem. 2, 540 (1963).

35. Bader, R. F. W. and Huang, K. P., J. Chem. Phys. 43, 3760 (1965).

36. Reddoch, A. H., J. Chem. Phys. 35, 1085 (1961).

37. Gaunt, J. and Ainscough, J. G., Spectrochim. Acta 10, 52 (1957).

38. Carlson, G. L., Spectrochim. Acta 19, 1291 (1963).

39. Bader, R. F. W. and Westland, H. D., Can. J. Chem. 39, 2306 (1961).

40. Haarhoff, P. C. and Pistorius, C. F. W. T., Z. Naturforsch. 14A, 972 (1959).

41. Brunvall, J., Acta Chem. Scand. 21, 473 (1967).

42. Walton, R. A. and Brisdon, B. J., J. Chem. Soc. I967A, 2489 (1967).

43. Fleming, P. B. Preparation and spectra of some lower hexanuclear niobium halide cluster compounds. Unpublished Ph.D. thesis. Ames, Iowa, Library, Iowa State University. 1968.

44. Hogue, R. D. Reactions and characterization of compounds containing tungsten halide cluster species. Unpublished Ph.D. thesis. Ames, Iowa, Library, Iowa State University. 1968.

45. Meloche, V. W., Martin, R. L. and Webb, W. H., Anal. Chem. 29, 527 (1957).

46. Wagner, E. L. and Hornig, D. F., J. Chem. Phys. 18, 296 (1950).

47. Linevsky, M. J., J. Chem. Phys. 34, 587 (1961).

48. Cotton, F. A. Chemical applications of group theory. New York, New York, Interscience Publishers, Inc. 1964.

49. Herzberg, G. Infrared and Raman spectra of polyatomic molecules. New York, New York, D. Van Nostrand Company, Inc. 1945.

50. Nakamoto, K. Infrared spectra of inorganic and coordination compounds. New York, New York, John Wiley and Sons, Inc. 1963.

51. Dennison, D. M., Phil. Mag. 1, 195 (1926).

52. Simanouti, T., J. Chem. Phys. 17, 245 (1949).

53. Wilson, E. B., J. Chem. Phys. 7, 1047 (1939).

54. Wilson, E. B., J. Chem. Phys. 9, 76 (1941).

55. Wilson, E. B. and Crawford, B. L., J. Chem. Phys. 6, 223 (1938).

56. Howard, J. B. and Wilson, E. B., J. Chem. Phys. 2, 630 (1934).

57. Meister, A. G. and Cleveland, F. F., Am. J. Phys. 14, 13 (1946).

58. Kilpatrick, J. E., J. Chem. Phys. 16, 749 (1948).

59. Nielsen, J. R. and Berryman, L. H., J. Chem. Phys. 17, 659 (1949).

60. Wilson, E. B., Decius, J. C. and Cross, P. C. Molecular vibrations. New York, New York, McGraw-Hill Book Company, Inc. 1955.

61. Ogawa, T. and Miyazawa, T., Spectrochim. Acta 20, 557 (1964).

62. Onishi, T. and Shimanouchi, T., Spectrochim. Acta 20, 325 (1964).

63. Beattie, I. R., Gilson, T. and Cocking, P., J. Chem. Soc. 1967A, 702 (1967).

64. Adams, D. M., Chandler, P. J. and Churchill, R. G., J. Chem. Soc. 1967A, 1272 (1967).

65. Adams, D. M. and Churchill, R. G., J. Chem. Soc. 1968A, 2141 (1968).

66. Pauling, L. The nature of the chemical bond. 3rd ed. Ithaca, New York, Cornell University Press. 1960.

67. Sun, C. E., Parr, R. G. and Crawford, B. L., J. Chem. Phys. 17, 840 (1949).

68. Decius, J. C., J. Chem. Phys. 17, 1315 (1949).

69. Decius, J. C., J. Chem. Phys. 16, 1025 (1948).

70. Polo, S. R., J. Chem. Phys. 24, 1133 (1956).

71. Mann, D. E., Shimanouchi, T., Meal, J. H. and Fano, L., J. Chem. Phys. 27, 43 (1957).

72. Mann, D. E., Fano, L., Meal, J. H. and Shimanouchi, T., J. Chem. Phys. 27, 51 (1957).

73. Overend, J. and Scherer, J. R., J. Chem. Phys. 32, 1289 (1960).

74. Overend, J. and Scherer, J. R., J. Chem. Phys. 32, 1296 (1960).

75. Overend, J. and Scherer, J. R., J. Chem. Phys. 32, 1720 (1960).

76. Aldous, J. and Mills, I. M., Spectrochim. Acta 18, 1073 (1962).

77. Freeman, J. M. and Henshall, T., J. Mol. Spectry. 25, 101 (1968)

78. Bruton, M. J. and Woodward, L. A., Spectrochim. Acta 23A, 175 (1967).

79. Needham, C. D. and Overend, J., Spectrochim. Acta 22, 1383 (1966).

80. Mann, D. E., Fano, L., Cahill, J. and Shimanouchi, T., J. Chem. Phys. 22, 764 (1954).

81. Miyazawa, T., J. Chem. Phys. 29, 246 (1958).

82. Schachtschneider, J. H. and Snyder, R. G., Spectrochim. Acta 19, 117 (1963).

83. Hunziker, H., J. Mol. Spectry. 17, 131 (1965).

84. Givens, W. R. Numerical computation of the characteristic values of a real symmetric matrix. Oak Ridge National Laboratory Report 1574. 1954.

85. Adams, D. M. and Chandler, P. J., Chem. Commun. 1966, 69 (1966).

86. Adams, D. M. Metal-ligand and related vibrations. New York, New York, St. Martin's Press. 1968.

87. Colthup, N. B., Daley, L. H. and Wiberly, S. E. Introduction to infrared and Raman spectroscopy. New York, New York, Academic Press, Inc. 1964.

88. Beattie, I. R., Gilson, T. R. and Ozin, G. A., J. Chem. Soc. 1968A, 2765 (1968).

89. El-Sayed, M. A. and Kaesz, H. D., Inorg. Chem. 2, 158 (1963).

90. Adams, D. M. and Lock, P. J., J. Chem. Soc. 1967A, 620 (1967).

91. Hiraishi, J., Nakagawa, I. and Shimanouchi, T., Spectrochim. Acta 20, 819 (1964).

92. Woodward, L. A. and Ware, M. J., Spectrochim. Acta 20, 711 (1964).

93. Scrocco, M., Spectrochim. Acta 22, 201 (1966).

94. Colton, R. The chemistry of rhenium and technetium. Sydney, Australia, John Wiley and Sons, Ltd. 1965.

95. Schäfer, H. and Schnering, H. G., Angew. Chem. 76, 833 (1964).

96. Schäfer, H., Schnering, H. G., Tillack, J., Kühnen, F., Wohrle, H. and Bauman, H., Z. anorg. allgem. Chem. 353, 281 (1967).

97. Bateman, L. R., Blount, J. F. and Dahl, L. F., J. Am. Chem. Soc. 88, 1082 (1966).

98. Schäfer, H., Schnering, H. G., Neihues, K. J. and Nieder-Vahrenholz, H. G., J. Less Common Metals 9, 95 (1965).

99. Morino, Y. and Kuchitsu, J., J. Chem. Phys. 20, 1809 (1952).

100. Perlis, S. Theory of matrices. Reading, Massachusetts, Addison-Wesley Publishing Company, Inc. 1952.

101. Barrow, G. M. Introduction to molecular spectroscopy. New York, New York, McGraw-Hill Book Company, Inc. 1962.

ACKNOWLEDGEMENTS

The author expresses his thanks to Dr. Robert E. McCarley whose guidance and encouragement throughout the period of graduate study has made this work possible.

Special thanks are also due the members, both past and present, of physical and inorganic chemistry group X for their magnanimous exchange of equipment, ideas and criticism: to Mr. John Meyer for the molybdenum and tantalum compounds; to Dr. Ronald Hogue for the tungsten compounds; to Dr. Peter Fleming for the niobium compounds; to Dr. Peter Kilty for furnishing the infrared cells, and to Miss Evelyn Conrad for helpful suggestions concerning the spectrophotometric equipment.

This section would not be complete without a special note of thanks to the author's parents for their patient understanding and support throughout the years of education.

APPENDIX A: VIBRATIONAL SECULAR EQUATION

The potential (V) and kinetic (T) energies of molecular vibration can be expressed in terms of mass weighted cartesian displacement coordinates (q_i) as

$$2V = \sum_{i=1}^{3N} \sum_{j=1}^{3N} f_{ij} q_i q_j \qquad (1A)$$

$$2T = \sum_{i=1}^{3N} \dot{q}_i^2 \qquad (2A)$$

where $f_{ij} = f_{ji} = (\partial^2 V/\partial q_i \partial q_j)_o$ and $\dot{q}_i = dq_i/dt$.

The Lagrangian equation of motion is

$$d/dt(\partial L/\partial \dot{q}_i) - (\partial L/\partial q_i) = 0 \qquad (3A)$$

where L = T-V. Since T is a function of velocities ($\dot{q}_i$) and V a function of the coordinates (q_i) only, Equation (3A) can be rewritten as

$$d/dt(\partial T/\partial \dot{q}_i) - (\partial V/\partial q_i) = 0 \; . \qquad (4A)$$

Substitution of the expressions for V and T into Equation (4A) results in a set of differential equations

$$\ddot{q}_j + \sum_{i=1}^{3N} f_{ij} q_i = 0 \qquad j = 1, 2, 3\text{----}3N \qquad (5A)$$

where $\ddot{q}_j = d^2(q_j)/dt^2$. One possible type of solution is

$$q_i = A_i \cos(\lambda^{\frac{1}{2}} t + \epsilon) \qquad (6A)$$

where A_i, λ and ϵ are constants. Substituting this solution into the differential equations (5A) produces a set of simultaneous homogeneous linear algebraic equations

$$\sum_{i=1}^{3N} (f_{ij}-\delta_{ij}\lambda)A_i = 0 \qquad j = 1, 2\text{----}3N \qquad (7A)$$

where $\delta_{ij} = 1(i=j), 0(i\neq j)$. According to Cramer's rule (100), nontrivial values of λ are those which satisfy the determinental or secular equation

$$\begin{vmatrix} f_{11}-\lambda & f_{12}\text{----------}f_{1,3N} \\ f_{21} & f_{22}-\lambda\text{--------}f_{2,3N} \\ f_{31} & \\ & \\ & \\ f_{3N,1} & f_{3N,2}\text{--------}f_{3N,3N}-\lambda \end{vmatrix} = 0 \qquad (8A)$$

where $\lambda = 4\pi^2c^2\bar{\upsilon}^2$ and $\bar{\upsilon}$ (wavenumber) = υ/c.

APPENDIX B: RELATION OF G MATRIX AND KINETIC ENERGY

The matrix expression for the kinetic energy of vibration, expressed in terms of the 3N-6 internal coordinates, is

$$2T = \dot{R}^T G^{-1} \dot{R} \tag{1B}$$

where the matrix G is related to the various atomic masses and coordinates in a molecule composed of N atoms.

The kinetic energy of vibration, T, can also be expressed in terms of the mass weighted cartesian displacement coordinates, q_i, as

$$2T = \dot{q}^T \dot{q} \tag{2B}$$

where $\dot{q} = \text{col}(\dot{q}_1, \dot{q}_2 \text{---} \dot{q}_{3N})$. The internal coordinates, R_i, are related to the mass weighted cartesian displacement coordinates, q_i, by the matrix expression

$$R = Dq \tag{3B}$$

where $R = \text{col}(R_1, R_2 \text{---} R_{3N-6})$ and $q = \text{col}(q_1, q_2 \text{---} q_{3N})$. It remains then to find the inverse transformation of Equation (3B) and substitute the time derivative form into Equation (2B) and derive the expression for the G matrix in Equation (1B). The transformation matrix D is, however, a 3N-6X3N matrix and as such is singular and does not possess a unique inverse (100). This difficulty, however, can be overcome by employing certain algebraic matrix techniques (101).

The matrix D can be made square by adding six additional rows, D_o, which represent the six conditions of zero translational and zero angular momentum

$$d = \begin{pmatrix} D \\ D_o \end{pmatrix} \tag{4B}$$

and $$d^{-1} = (Z\ Z_o) \tag{5B}$$

where d and d^{-1} are square 3NX3N matrices, Z is a 3NX3N-6 matrix and Z_o is a 3NX6 matrix. The column vector, designated as P, representing the internal coordinates, can then be presented in a more usable matrix form which is expressed as

$$P = \begin{pmatrix} R \\ r \end{pmatrix} = \begin{pmatrix} D \\ D_o \end{pmatrix} q = dq\ . \tag{6B}$$

From the definition of internal coordinates $r = D_o q$ is a column vector having six zero elements. The inverse transformation of Equation (6B) can be formulated as

$$q = d^{-1}P \tag{7B}$$

or in time derivative form as

$$\dot{q} = d^{-1}\dot{P} \qquad \text{where } \dot{P} = \begin{pmatrix} \dot{R} \\ \dot{r} \end{pmatrix} \tag{8B}$$

Substitution of Equation (8B) into Equation (2B) results in the matrix expression for the kinetic energy as

$$2T = \dot{P}^T(d^{-1})^T d^{-1}\dot{P}\ . \tag{9B}$$

This expression can be expanded in terms of its component matrices.

$$2T = (\dot{R}^T \dot{r}^T)\begin{pmatrix} Z^T \\ Z_o^T \end{pmatrix}(Z\ Z_o)\begin{pmatrix} \dot{R} \\ \dot{r} \end{pmatrix} \tag{10B}$$

$$2T = (\dot{R}^T Z^T + \dot{r}^T Z_o^T)(Z\dot{R} + Z_o\dot{r}) \tag{11B}$$

$$2T = \dot{R}^T Z^T Z\dot{R} + \dot{R}^T Z^T Z_o\dot{r} + \dot{r}^T Z_o^T Z\dot{R} + \dot{r}^T Z_o^T Z_o\dot{r} \tag{12B}$$

Since r is a zero matrix, $\dot{r}$ is also and therefore the last three terms in Equation (12B) are zero and the desired reduction to 3N-6 order matrices has been completed. The resultant matrix expression for T is

$$2T = \dot{R}^T Z^T Z\dot{R} \tag{13B}$$

where the product matrix Z^TZ has dimension 3N-6. The Z matrix can be expressed in more convenient terms by noting that it occurs in the inverse of d

$$dd^{-1} = \begin{pmatrix} D \\ D_o \end{pmatrix} (Z\ Z_o) = \begin{pmatrix} DZ & DZ_o \\ D_oZ & D_oZ_o \end{pmatrix} = E(3N\text{X}3N) \tag{14B}$$

where E is the 3NX3N unit matrix. From this expression it follows that

$$DZ = E(3N\text{-}6\text{X}3N\text{-}6) \tag{15B}$$

A second expression which is useful is

$$d^{-1}d = (Z\ Z_o)\begin{pmatrix} D \\ D_o \end{pmatrix} = E(3N\text{X}3N) \tag{16B}$$

or

$$(ZD + Z_oD_o) = E(3N\text{X}3N) \tag{17B}$$

If the transpose of Equation (17B) is taken, there results a matrix expression

$$(D^TZ^T + D_o^TZ_o^T) = E(3N\text{X}3N) \tag{18B}$$

When this equation is left multiplied by the matrix D and

right multiplied by the matrix Z, there results a dimension reduction.

$$DD^TZ^TZ + DD_o^TZ_o^TZ = DZ = E(3N\text{-}6X\ 3N\text{-}6) \tag{19B}$$

Since the internal coordinates are orthogonal to the over-all translational and rotational coordinates, it follows that D and D_o are orthogonal matrices and therefore it follows that

$$DD_o^T = 0 \tag{20B}$$

where 0 is the zero matrix. This eliminates the second term in Equation (19B) and produces the matrix expressions

$$DD^TZ^TZ = E \tag{21B}$$

or

$$Z^TZ = (DD^T)^{-1} . \tag{22B}$$

When this last expression is substituted into matrix Equation (13B), the kinetic energy can be rewritten in more convenient terms.

$$2T = \dot{R}^T(DD^T)^{-1}\dot{R} \tag{23B}$$

Comparing this result with the original matrix expression (1B) for the kinetic energy of vibration, it follows that

$$G^{-1} = (DD^T)^{-1} \tag{24B}$$

or

$$G = DD^T \tag{25B}$$

where it is observed that the G matrix is simply related to the transformation matrix D between the mass weighted cartesian displacement coordinates and the internal coordinates.

APPENDIX C: NORMAL COORDINATES

In order to study molecular vibrations by means of a quantum mechanical treatment, it is necessary to simplify the mathematics involved and introduce a new set of coordinates, Q_k; k = 1, 2---3N, called normal coordinates. There is one normal coordinate associated with each normal mode of motion. The normal coordinates are linear combinations of the mass weighted cartesian displacement coordinates

$$Q = \ell' q \tag{1C}$$

where $Q = \mathrm{col}(Q_k)$, $q = \mathrm{col}(q_k)$ and ℓ' is the transformation matrix. The transformation matrix ℓ' is chosen such that the potential and kinetic energies of vibration contain no cross products when they are expressed in terms of the normal coordinates.

$$2T = \sum_{k=1}^{3N} \dot{Q}_k^2 \tag{2C}$$

$$2V = \sum_{k=1}^{3N} \lambda_k Q_k^2 \tag{3C}$$

Using these normal coordinates and eliminating those involving translation and rotation, the Schrödinger wave equation for the molecular vibrations of a nonlinear polyatomic molecule can be written (60) as

$$(-\hbar^2/2 \sum_{i=1}^{3N-6} \partial^2/\partial Q_i^2 + 1/2 \sum_{i=1}^{3N-6} \lambda_i Q_i^2)\Psi_T = E\Psi_T \tag{4C}$$

The wavefunction of the complete system, Ψ_T is considered separable into individual wavefunctions, each involving the various normal coordinates.

$$\Psi_T = \psi_1(Q_1) \cdot \psi_2(Q_2) \cdot \psi_3(Q_3) \text{-----} \psi_{3N-6}(Q_{3N-6}) \qquad (5C)$$

When this is done, it can be seen that the system wave equation (4C) is satisfied if the functions $\psi_k(Q_k)$ satisfy similar wave equations of the type

$$(-\hbar^2/2\ d^2/dQ_k^2 + 1/2\lambda_k Q_k^2)\ \psi_k(Q_k) = E_k\ \psi_k(Q_k) \qquad (6C)$$

where E_k is the energy associated with $\psi_k(Q_k)$ and k = 1, 2, 3---3N-6. The system energy, E_T, can then be expressed as a sum of these individual energies.

$$E_T = \sum_{k=1}^{3N-6} E_k \qquad (7C)$$

Each of the values of the energies E_k, associated with a particular normal coordinate $\psi_k(Q_k)$, has related to it a quantum number, v_k, and a vibrational frequency, υ_k, such that

$$E_k = (v_k + 1/2)h\upsilon_k$$

This frequency υ_k is known as the normal vibrational frequency.

APPENDIX D: USE OF SYMMETRY COORDINATES IN FACTORING G AND F MATRICES

The potential (V) and kinetic (T) energies of vibration, expressed in terms of the internal coordinates, R_k, can be written in matrix form as

$$2V = R^T F R \tag{1D}$$

$$2T = \dot{R}^T G^{-1} \dot{R} \tag{2D}$$

$$R = LQ \tag{3D}$$

where Q represents the column vector of normal coordinates, Q_k. The internal symmetry coordinates, S_k, are related to the internal coordinates, R_k, by an orthogonal linear transformation matrix U.

$$S = UR \tag{4D}$$

or

$$R = U^{-1} S \tag{5D}$$

When this last expression is substituted into Equations (1D) and (2D), there results the equations

$$2V = S^T (U^{-1})^T F U^{-1} S \tag{6D}$$

$$2T = \dot{S}^T (U^{-1})^T G^{-1} U^{-1} \dot{S} \tag{7D}$$

$$S = L'Q \tag{8D}$$

where $$L' = UL \tag{9D}$$

Substitution of the values of S expressed in the matrix equation (8D) into Equations (6D) and (7D) results in the following expressions

$$2V = Q^T(L')^T(U^{-1})^T F U^{-1} L' Q \tag{10D}$$

$$2T = \dot{Q}^T(L')^T(U^{-1})^T G^{-1} U^{-1} L' \dot{Q} \tag{11D}$$

Since U is an orthogonal matrix, $U^T = U^{-1}$ and the last two expressions can be rewritten in the form

$$2V = Q^T(L')^T U F U^T L' Q \tag{12D}$$

$$2T = \dot{Q}^T(L')^T U G^{-1} U^T L' \dot{Q} \tag{13D}$$

According to the definition of the normal coordinate, no cross products are to occur in the potential or kinetic energies when expressed in terms of these coordinates. This definition, expressed in matrix form is

$$2V = Q^T \Lambda Q \tag{14D}$$

$$2T = \dot{Q}^T E \dot{Q} \tag{15D}$$

where $\Lambda = \text{diag}(4\pi^2 \upsilon_k^2)$ and E = identity matrix. Comparing these expressions with the Equations (12D) and (13D), it is obvious that

$$\Lambda = (L')^T U F U^T (L') \tag{16D}$$

$$E = (L')^T U G^{-1} U^T (L') \tag{17D}$$

$$\text{or} \quad (L')^T = (L')^{-1}[U G^{-1} U^T]^{-1} \tag{18D}$$

Upon substitution of this last expression into Equation (16D), the following series of matrix equations is obtained

$$\Lambda = (L')^{-1}[U G^{-1} U^T]^{-1} U F U^T (L') \tag{19D}$$

$$\Lambda = (L')^{-1}[U G U^T][U F U^T](L') \tag{20D}$$

$$\text{or} \quad [U G U^T][U F U^T](L') = (L')\Lambda \tag{21D}$$

Equation (21D) represents the characteristic equation of vibration which has been factored to the maximum extent made possible by the symmetry. It can also be expressed in the form

$$(G'F')L' = L'\Lambda \tag{22D}$$

$$G' = UGU^T \tag{23D}$$

$$F' = UFU^T \tag{24D}$$

where G' and F' represent the symmetry factored kinetic energy and potential energy matrices respectively.

APPENDIX E: KINETIC ENERGY MATRIX ELEMENTS OF M_2X_{10}

The following notation was used to describe the values of the unfactored kinetic energy matrix elements, g_{ij}, associated with the M_2X_{10} molecule of D_{2h} symmetry. The eight molecular parameters are represented as

μ_m = 1/mass of metal atom

μ_X = 1/mass of halogen atom

A = X(axial)-M-X(axial) angle

B = X(equat.)-M-X(equat.) angle

C = M-X(bridge)-M angle

X = 1/d(M-X(axial))

Z = 1/d(M-X(bridge))

where d represents the various metal-halogen distances. The related identities were also employed

$D = 180^\circ - C$

$E = 1/2(180^\circ - B + C)$

$F = D + E$

$\cos H = \cos(A/2)\cos(D/2)$

$\cos K = \cos(180^\circ - A/2)\cos(B/2)$

$\sin H = (1-\cos^2 H)^{\frac{1}{2}}$

$\sin K = (1-\cos^2 K)^{\frac{1}{2}}$

Table 16. Kinetic energy matrix elements of M_2X_{10}

$g_{ss} = \mu_m + \mu_x$

$g'_{ss} = \mu_m \cdot \cos A$

$g_{tt} = \mu_m + \mu_x$

$g'_{tt} = \mu_m \cdot \cos B$

$g_{rr} = \mu_m + \mu_x$

$g'_{rr} = \mu_x \cdot \cos C$

$g''_{rr} = \mu_m \cdot \cos D$

$g_{\gamma\gamma} = (X^2+Z^2)\mu_x + (X^2+Z^2-2XZ \cdot \cos E)\mu_m$

$g'_{\gamma\gamma} = ((\cos D-2\cos E \cdot \cos F+\cos B \cdot \cos^2 E)X^2 +$
$2(\cos F-\cos D \cdot \cos E-\cos B \cdot \cos E+\cos^2 E \cdot \cos F)XZ +$
$(\cos B-2\cos E \cdot \cos F+\cos D \cdot \cos^2 E)Z^2)\mu_m/\sin^2 E$

$g''_{\gamma\gamma} = -Z^2\mu_x \cos C$

$g_{\alpha\alpha} = 2X^2\mu_x + 2X^2(1-\cos B)\mu_m$

$g_{uu} = (Y^2+Z^2)\mu_x + (Y^2+Z^2-2YZ \cdot \cos H)\mu_m$

$g'_{uu} = (Y^2(\cos D-\cos^2 H)/\sin^2 H)\mu_x + ((Y-2Z \cdot \cos H)Y(\cos D-$
$\cos^2 H)/\sin^2 H + \sin^2 H(1-((\cos D-\cos^2 H)/\sin^2 H)^2) +$
$\cos D(\cos D-\cos^2 H)/\sin^2 H)Z^2)\mu_m$

$g''_{uu} = ((\cos D-2\cos^2 H+\cos A\cos^2 H)Y^2 + 2(\cos H-\cos D \cdot \cos H-$
$\cos A \cdot \cos H+\cos^3 H)YZ + (\cos A-2\cos^2 H+\cos D \cdot \cos^2 H)Z^2) \cdot$
$\mu_m/\sin^2 H$

$g'''_{uu} = (Z^2(\cos A-\cos^2 H)/\sin^2 H)\mu_x + ((Z-2Y\cos H)Z(\cos A-$
$\cos^2 H)/\sin^2 H + (\sin^2 H(1-((\cos A-\cos^2 H)/\sin^2 H)^2) +$
$\cos A(\cos A-\cos^2 H)/\sin^2 H)Y^2)\mu_m$

$g^{IV}_{uu} = -(\sin^2 H+\cos^2 H \cdot \cos C)Z^2\mu_x$

Table 16. (Continued)

$g^{V}_{uu} = -(\sin^2H+\cos^2H\cdot\cos C)Z^2\mu_x$

$g_{vv} = (X^2+Y^2)\mu_x + (X^2+Y^2-2XY\cdot\cos K)\mu_m$

$g'_{vv} = (Y^2(\cos B-\cos^2K)/\sin^2K)\mu_x + ((Y-2X\cdot\cos K)Y(\cos B-\cos^2K)/\sin^2K + (\sin^2K(1-((\cos B-\cos^2K)/\sin^2K)^2) + \cos B(\cos B-\cos^2K)/\sin^2K)X^2)\mu_m$

$g''_{vv} = (X^2(\cos A-\cos^2K)/\sin^2K)\mu_x + ((X-2Y\cos K)X(\cos A-\cos^2K)/\sin^2K + (\sin^2K(1-((\cos A-\cos^2K)/\sin^2K)^2) + \cos A(\cos A-\cos^2K)/\sin^2K)Y^2)\mu_m$

$g'^{\prime\prime}_{vv} = ((\cos A-2\cos^2K+\cos B\cos^2K)X^2 + 2(\cos K-\cos A\cdot\cos K-\cos B\cdot\cos K+\cos^3K)XY + (\cos B-2\cos^2K+\cos A\cdot\cos^2K)Y^2)\mu_m/\sin^2K$

$g_{\alpha\alpha} = 2X^2\mu_x + 2X^2(1-\cos B)\mu_m$

$g_{st} = \mu_m\cos K$

$g_{sr} = \mu_m\cos H$

$g_{su} = -Z\mu_m\sin H$

$g'_{su} = -(Z\cdot\sin H(\cos A-\cos^2H)/\sin^2H + Y\sin A(\cos H-\cos A\cdot\cos H)/\sin A\cdot\sin H)\mu_m$

$g_{sv} = -X\mu_m\sin K$

$g'_{sv} = -(X\cdot\sin K(\cos A-\cos^2K)/\sin^2K + Y\cdot\sin A(\cos K-\cos A\cdot\cos K)/\sin A\cdot\sin K)\mu_m$

$g_{s\alpha} = -(X\cdot\sin K(\cos K-\cos K\cdot\cos B)/\sin K\cdot\sin B + X\sin K(\cos K-\cos K\cdot\cos B)/\sin K\cdot\sin B)\mu_m$

$g_{tr} = \mu_m\cos E$

$g'_{tr} = \mu_m\cos F$

$g_{t\gamma} = -Z\mu_m\sin E$

Table 16. (Continued)

$$g'_{t\gamma} = -(X\cdot \sin B(\cos F-\cos B\cdot\cos E)/\sin B\cdot\sin E + Z\cdot\sin F(\cos B-\cos F\cdot\cos E)/\sin F\cdot\sin E)\mu_m$$

$$g_{t\alpha} = -X\mu_m \sin B$$

$$g_{tu} = -(Y\cdot\sin K(\cos E-\cos K\cdot\cos H)/\sin K\cdot\sin H + Z\cdot\sin E(\cos K-\cos E\cdot\cos H)/\sin E\cdot\sin H)\mu_m$$

$$g'_{tu} = -(Y\cdot\sin K(\cos F-\cos K\cdot\cos H)/\sin K\cdot\sin H + Z\cdot\sin F(\cos K-\cos F\cdot\cos H)/\sin F\cdot\sin H)\mu_m$$

$$g_{r\gamma} = -X\mu_m \sin E$$

$$g'_{r\gamma} = -(X\cdot\sin F(\cos D-\cos F\cdot\cos E)/\sin F\cdot\sin E + Z\cdot\sin D(\cos F-\cos D\cdot\cos E)/\sin D\cdot\sin E)\mu_m$$

$$g''_{r\gamma} = -Z\mu_x \sin E$$

$$g_{r\alpha} = -(X\cdot\sin E(\cos F-\cos B\cdot\cos E)/\sin B\cdot\sin E + X\cdot\sin F(\cos E-\cos F\cdot\cos B)/\sin F\cdot\sin B)\mu_m$$

$$g_{ru} = -Y\mu_m \sin H$$

$$g'_{ru} = -(Y\sin H(\cos D-\cos^2 H)/\sin^2 H + Z\cdot\sin D(\cos H-\cos D\cdot\cos H)/\sin D\cdot\sin H)\mu_m$$

$$g''_{ru} = Z\mu_x \sin C\cdot\cos H$$

$$g_{\gamma u} = (Z^2(\cos K-\cos E\cdot\cos H)/\sin E\cdot\sin H)\mu_x + ((Z-X\cdot\cos E-Y\cdot\cos H)Z\cdot(\cos K-\cos E\cdot\cos H)/\sin E\cdot\sin H + (\sin E\cdot\sin H(1-((\cos K-\cos E\cdot\cos H)/\sin E\cdot\sin H)^2) + \cos K(\cos K-\cos E\cdot\cos H)/\sin E\cdot\sin H)\cdot XY)\mu_m$$

$$g'_{\gamma u} = ((\cos D-\cos^2 H-\cos E\cdot\cos F+\cos E\cdot\cos H\cdot\cos K)XY + (\cos H-\cos D\cdot\cos H-\cos E\cdot\cos K+\cos E\cdot\cos F\cdot\cos H)XZ + (\cos F-\cos H\cdot\cos K-\cos D\cdot\cos E + \cos E\cdot\cos^2 H)YZ +$$

Table 16. (Continued)

$(\cos K-\cos F\cdot\cos H-\cos E\cdot\cos H+\cos D\cdot\cos E\cdot\cos H)Z^2)\cdot$
$\mu_m/(\sin E\cdot\sin H)$

$g''_{\gamma u} = Z^2\mu_x\cos C\cdot\cos H$

$g_{\alpha u} = ((\cos E+\cos F-\cos B\cdot\cos F-\cos B\cdot\cos E-2\cos H\cos K+2\cos B\cdot\cos H\cdot$
$\cos K)XY + (2\cos K-2\cos B\cdot\cos K-\cos F\cdot\cos H-\cos E\cdot\cos H+\cos B\cdot$
$\cos E\cos H+\cos B\cdot\cos F\cdot\cos H)XZ)\mu_m/(\sin B\cdot\sin H)$

$g_{uv} = (Y^2(\cos F-\cos K\cdot\cos H)/\sin K\cdot\sin H)\mu_x + ((Y-X\cdot\cos K-Z\cdot\cos H)Y\cdot$
$(\cos F-\cos K\cdot\cos H)/\sin K\cdot\sin H+(\sin K\cdot\sin H(1-((\cos F-\cos K\cdot$
$\cos H)/\sin K\cdot\sin H)^2) + \cos F(\cos F-\cos K\cdot\cos H)/\sin K\cdot\sin H)$
$XZ)\mu_m$

$g'_{uv} = (Y^2(\cos E-\cos K\cdot\cos H)/\sin K\cdot\sin H)\mu_x + ((Y-X\cdot\cos K-Z\cdot\cos H)Y\cdot$
$(\cos E-\cos K\cdot\cos H)/\sin K\cdot\sin H + (\sin K\cdot\sin H(1-((\cos E-\cos K\cdot$
$\cos H)/\sin K\cdot\sin H)^2) + \cos E(\cos E-\cos K\cdot\cos H)/\sin K\cdot\sin H)\cdot$
$XZ)\mu_m$

$g''_{uv} = ((\cos H-\cos F\cdot\cos K-\cos A\cdot\cos H+\cos H\cdot\cos^2 K)XY + (\cos F-2\cos H\cdot$
$\cos K+\cos A\cdot\cos H\cdot\cos K)Y^2 + (\cos A-\cos^2 K-\cos^2 H+\cos F\cdot\cos H\cdot$
$\cos K)XZ + (\cos K-\cos A\cdot\cos K-\cos H\cdot\cos F+\cos^2 H\cdot\cos K)YZ)\mu_m/$
$(\sin H\cdot\sin K)$

$g'''_{uv} = ((\cos H-\cos E\cdot\cos K-\cos A\cdot\cos H+\cos H\cdot\cos^2 K)XY +$
$(\cos E -2\cos H\cdot\cos K+\cos A\cdot\cos H\cdot\cos K)Y^2 + (\cos A-$
$\cos^2 K - \cos^2 H + \cos E\cdot\cos H\cdot\cos K)XZ + (\cos A-\cos A\cdot\cos K-$
$\cos E\cdot\cos H+\cos^2 H\cdot\cos K)YZ)\mu_m/(\sin H\cdot\sin K)$

APPENDIX F: VIBRATIONAL POTENTIAL ENERGY DISTRIBUTION

In order to establish the particular type or types of internal symmetry coordinates (or internal coordinates) associated with a fundamental vibrational frequency, it is necessary to calculate a potential energy distribution. Morino and Kuchitsu (99) have shown that a distribution of the potential energies of the internal symmetry coordinates (or internal coordinates) in the normal coordinates can serve as a representative measure of the band assignments.

The vibrational potential energy, V, can be expressed in terms of the internal symmetry coordinates in matrix form as

$$2V = S^T F' S \tag{1F}$$

$$\text{where} \quad S = L'Q \tag{2F}$$

The F' matrix represents the symmetry factored force constant matrix and L' is the transformation matrix between the normal coordinates, Q_n, and the internal symmetry coordinates, S_n. These two relationships can be combined and used to express the potential energy in terms of the normal coordinates.

$$2V = Q^T \left[(L')^T F' (L') \right] Q \tag{3F}$$

Employing the definition of the normal coordinates, and expanding Equation (3F), the potential energy of the whole molecule for a given vibration associated with a single normal coordinate, Q_n, can be written as

$$2V(Q_n) = Q_n^2 \sum_i \sum_j F'_{ij} L'_{in} L'_{jn} = Q_n^2 \lambda_n \tag{4F}$$

where $\lambda_n = 4\pi^2 \upsilon_n^2$. Since, in general, values of $F'_{ij}L'_{in}L'_{jn}$ are large when i = j, only the $F'_{ii}(L'_{in})^2$ terms are significant. These diagonal $F'_{ii}(L'_{in})^2$ terms represent the potential energy contributions to the normal coordinate from the internal symmetry coordinates. The general equation (4F) can be rewritten in another form which expresses the values of the potential energy distribution in more convenient terms.

$$\left[\sum_i \sum_j F'_{ij}L'_{in}L'_{jn} \right] / \lambda_n = 1 \qquad (5F)$$

With this relationship, it can be seen that terms of the type $F'_{ii}(L'_{in})^2\lambda_n^{-1}$ can be used to express the potential energy distribution on a percentage basis in a generalized valence force field ($F'_{ij} = 0$, $i \neq j$). When off-diagonal terms are included in the force field, however, only relative values of $F'_{ii}(L'_{in})^2\lambda_n^{-1}$ are meaningful.

APPENDIX G: OBSERVED AND CALCULATED INFRARED FREQUENCIES OF M_2X_{10}

Values quoted are in units of wavenumbers ($cm.^{-1}$). The calculated frequencies represent those obtained from the "best set" of force constants. For purposes of calculation, the frequency associated with the $\upsilon_4(B_{1u})$ mode was chosen to have a value of 0.0 $cm.^{-1}$.

Table 17. Observed and calculated infrared frequencies ($cm.^{-1}$)

Assignment		Nb_2Cl_{10} obs.	Nb_2Cl_{10} calc.	Mo_2Cl_{10} obs.	Mo_2Cl_{10} calc.	Ta_2Cl_{10} obs.	Ta_2Cl_{10} calc.	W_2Cl_{10} obs.	W_2Cl_{10} calc.	Re_2Cl_{10} obs.	Re_2Cl_{10} calc.
B_{1u}	ν_1	423	422	412	420	411	420	398	396	404	403
	ν_2	171	175	172	175	164	164	166	164	168	170
	ν_3	116	119	117	119	119	119	121	119	118	120
	ν_4	0.0	0.0	0.0	0.0	0.0	0.0	0.0	0.0	0.0	0.0
B_{2u}	ν_5	400	403	380	397	385	391	365	370	369	379
	ν_6	365	365	347	346	364	364	334	334	350	349
	ν_7	251	259	276	275	251	253	283	280	276	276
	ν_8	197	200	214	216	200	200	203	202	216	215
	ν_9	154	152	159	152	148	153	148	154	157	157
B_{3u}	ν_{10}	412	408	391	385	402	400	379	369	393	381
	ν_{11}	223	222	238	241	225	219	247	247	255	255
	ν_{12}	142	135	143	142	138	133	141	140	148	142
	ν_{13}	73	75	75	76	71	72	72	72	83	83

Table 17. (Continued)

Assignment		Nb_2Br_{10}		Ta_2Br_{10}		W_2Br_{10}		Ta_2I_{10}	
		obs.	calc.	obs.	calc.	obs.	calc.	obs.	calc.
B_{1u}	ν_1	299	295	261	260	260	259	197	197
	ν_2	112	117	112	115	114	117	83	83
	ν_3	77	80	79	81	73	75	61	61
	ν_4	0.0	0.0	0.0	0.0	0.0	0.0	0.0	0.0
B_{2u}	ν_5	263	283	244	246	244	254	176	191
	ν_6	219	218	217	217	212	212	155	154
	ν_7	159	152	162	162	179	175	107	106
	ν_8	127	127	127	128	129	130	95	95
	ν_9	105	97	102	99	103	97	77	70
B_{3u}	ν_{10}	283	282	251	249	253	247	186	187
	ν_{11}	145	143	147	148	158	159	116	109
	ν_{12}	96	91	96	92	95	93	73	77
	ν_{13}	63	63	63	63	63	63	45	45

APPENDIX H: VIBRATIONAL POTENTIAL ENERGY DISTRIBUTIONS IN M_2X_{10}

The relative values of $F'_{ii}(L'_{in})^2\lambda_n^{-1}$ are given in the following tables for the dimeric pentahalides: Nb_2Cl_{10}, Nb_2Br_{10}, Ta_2Cl_{10}, Ta_2Br_{10}, Ta_2I_{10}, Mo_2Cl_{10}, W_2Cl_{10}, W_2Br_{10} and Re_2Cl_{10}. The infrared vibrational frequencies ($\overline{\nu}$(calc.)) represent those generated by the "best set" of force constants for that particular molecule. The symmetry coordinate $\upsilon_4(B_{1u})$ has been purposely omitted since, by definition, it corresponds to a vibrational mode of zero frequency and therefore $F'_{ii} = 0$.

Table 18. Relative values of $F'_{ii}(L'_{in})^2\lambda_n^{-1}$ for niobium(V) chloride

Symmetry coordinate		Nb_2Cl_{10}($\bar{\upsilon}$ (calc.))				
		422	175	119		
B_{1u}	ν_1	1.000	0.044	0.035		
	ν_2	0.055	1.000	0.015		
	ν_3	0.025	0.026	1.000		
		403	365	259	200	152
B_{2u}	ν_5	1.000	0.094	0.389	0.012	0.005
	ν_6	0.134	1.000	0.005	0.000	0.000
	ν_7	0.143	0.005	1.000	0.409	0.081
	ν_8	0.095	0.003	0.255	1.000	0.134
	ν_9	0.084	0.003	0.176	0.031	1.000
		408	222	135	75	
B_{3u}	ν_{10}	1.000	0.135	0.014	0.000	
	ν_{11}	0.059	1.000	0.053	0.298	
	ν_{12}	0.027	0.026	1.000	0.029	
	ν_{13}	0.034	0.344	0.001	1.000	

Table 19. Relative values of $F'_{ii}(L'_{in})^2\lambda_n^{-1}$ for niobium(V) bromide

Symmetry coordinate		Nb_2Br_{10} ($\bar{\nu}$(calc.))				
		295	117	80		
	ν_1	1.000	0.159	0.088		
B_{1u}	ν_2	0.193	1.000	0.000		
	ν_3	0.082	0.019	1.000		
		283	218	152	127	97
	ν_5	1.000	0.033	1.000	0.108	0.005
	ν_6	0.123	1.000	0.002	0.001	0.000
B_{2u}	ν_7	0.596	0.011	0.916	0.351	0.159
	ν_8	0.366	0.006	0.046	1.000	0.388
	ν_9	0.453	0.007	0.128	0.128	1.000
		282	143	91	63	
	ν_{10}	1.000	0.820	0.039	0.000	
	ν_{11}	0.255	1.000	0.145	0.730	
B_{3u}	ν_{12}	0.138	0.028	1.000	0.120	
	ν_{13}	0.332	0.879	0.002	1.000	

Table 20. Relative values of $F'_{ii}(L'_{in})^2\lambda_n^{-1}$ for tantalum(V) chloride

Symmetry coordinate		Ta_2Cl_{10} ($\bar{\nu}$(calc.))				
		420	164	119		
	ν_1	1.000	0.007	0.020		
B_{1u}	ν_2	0.014	1.000	0.135		
	ν_3	0.010	0.144	1.000		
		391	364	253	200	153
	ν_5	1.000	0.045	0.082	0.006	0.003
	ν_6	0.045	1.000	0.002	0.000	0.000
B_{2u}	ν_7	0.036	0.000	1.000	0.235	0.056
	ν_8	0.022	0.000	0.168	1.000	0.078
	ν_9	0.019	0.000	0.113	0.026	1.000
		400	219	133	72	
	ν_{10}	1.000	0.037	0.006	0.000	
	ν_{11}	0.018	1.000	0.017	0.262	
B_{3u}	ν_{12}	0.008	0.007	1.000	0.017	
	ν_{13}	0.009	0.276	0.004	1.000	

Table 21. Relative values of $F'_{ii}(L'_{in})^2\lambda_n^{-1}$ for tantalum(V) bromide

Symmetry coordinate		Ta_2Br_{10} ($\bar{\nu}$(calc.))				
		260	115	81		
B_{1u}	ν_1	1.000	0.065	0.059		
	ν_2	0.087	1.000	0.016		
	ν_3	0.042	0.036	1.000		
		246	217	162	128	99
B_{2u}	ν_5	1.000	0.073	0.535	0.062	0.004
	ν_6	0.147	1.000	0.003	0.000	0.000
	ν_7	0.323	0.012	1.000	0.214	0.113
	ν_8	0.146	0.005	0.051	1.000	0.354
	ν_9	0.186	0.006	0.125	0.175	1.000
		249	148	92	63	
B_{3u}	ν_{10}	1.000	0.351	0.023	0.000	
	ν_{11}	0.132	1.000	0.093	0.524	
	ν_{12}	0.056	0.024	1.000	0.093	
	ν_{13}	0.137	0.689	0.001	1.000	

Table 22. Relative values of $F'_{ii}(L'_{in})^2\lambda_n^{-1}$ for tantalum(V) iodide

Symmetry coordinate		Ta_2I_{10} ($\bar{\nu}$(calc.))				
		197	83	61		
	ν_1	1.000	0.138	0.109		
B_{1u}	ν_2	0.176	1.000	0.001		
	ν_3	0.103	0.022	1.000		
		191	154	106	95	70
	ν_5	0.548	0.096	0.285	1.000	0.019
	ν_6	0.130	1.000	0.059	0.035	0.000
B_{2u}	ν_7	1.000	0.000	1.000	0.034	0.103
	ν_8	0.426	0.012	0.493	0.813	0.202
	ν_9	0.401	0.007	0.010	0.075	1.000
		187	109	77	45	
	ν_{10}	0.861	0.844	0.152	0.004	
	ν_{11}	1.000	1.000	0.047	0.021	
B_{3u}	ν_{12}	0.272	0.027	1.000	0.041	
	ν_{13}	0.313	0.099	0.007	1.000	

Table 23. Relative values of $F'_{ii}(L'_{in})^2\lambda_n^{-1}$ for molybdenum(V) chloride

Symmetry coordinate		Mo_2Cl_{10} ($\bar{\nu}$(calc.))				
		420	175	119		
	ν_1	1.000	0.037	0.038		
B_{1u}	ν_2	0.051	1.000	0.027		
	ν_3	0.025	0.040	1.000		
		397	346	275	216	152
	ν_5	1.000	0.057	0.468	0.045	0.008
	ν_6	0.094	1.000	0.006	0.001	0.000
B_{2u}	ν_7	0.347	0.005	1.000	0.111	0.059
	ν_8	0.136	0.002	0.037	1.000	0.106
	ν_9	0.115	0.002	0.049	0.048	1.000
		385	241	142	76	
	ν_{10}	1.000	0.164	0.019	0.001	
	ν_{11}	0.130	1.000	0.032	0.069	
B_{3u}	ν_{12}	0.034	0.008	1.000	0.030	
	ν_{13}	0.040	0.163	0.008	1.000	

Table 24. Relative values of $F'_{ii}(L'_{in})^2\lambda_n^{-1}$ for tungsten(V) chloride

Symmetry coordinate		W_2Cl_{10} ($\bar{\nu}$(calc.))				
		396	164	119		
	ν_1	1.000	0.006	0.026		
B_{1u}	ν_2	0.015	1.000	0.191		
	ν_3	0.011	0.202	1.000		
		370	334	280	202	154
	ν_5	1.000	0.010	0.155	0.017	0.004
	ν_6	0.002	1.000	0.035	0.000	0.000
B_{2u}	ν_7	0.123	0.019	1.000	0.044	0.036
	ν_8	0.030	0.001	0.019	1.000	0.094
	ν_9	0.031	0.001	0.038	0.065	1.000
		369	247	140	72	
	ν_{10}	1.000	0.063	0.008	0.000	
	ν_{11}	0.050	1.000	0.008	0.079	
B_{3u}	ν_{12}	0.011	0.002	1.000	0.015	
	ν_{13}	0.012	0.132	0.007	1.000	

Table 25. Relative values of $F'_{ii}(L'_{in})^2\lambda_n^{-1}$ for tungsten(V) bromide

Symmetry coordinate		W_2Br_{10} ($\bar{\nu}$(calc.))				
		259	117	75		
	ν_1	1.000	0.072	0.046		
B_{1u}	ν_2	0.089	1.000	0.013		
	ν_3	0.033	0.029	1.000		
		254	212	175	130	97
	ν_5	1.000	0.040	0.627	0.087	0.007
	ν_6	0.083	1.000	0.005	0.001	0.000
B_{2u}	ν_7	0.602	0.007	1.000	0.051	0.068
	ν_8	0.149	0.001	0.001	1.000	0.244
	ν_9	0.184	0.002	0.025	0.154	1.000
		247	159	93	63	
	ν_{10}	1.000	0.355	0.029	0.001	
	ν_{11}	0.251	1.000	0.064	0.151	
B_{3u}	ν_{12}	0.058	0.005	1.000	0.098	
	ν_{13}	0.133	0.297	0.023	1.000	

Table 26. Relative values of $F'_{ii}(L'_{in})^2\lambda_n^{-1}$ for rhenium(V) chloride

Symmetry coordinate		Re_2Cl_{10} ($\bar{\nu}$(calc.))				
		403	170	120		
	ν_1	1.000	0.007	0.024		
B_{1u}	ν_2	0.016	1.000	0.153		
	ν_3	0.012	0.163	1.000		
		379	349	276	215	157
	ν_5	1.000	0.025	0.137	0.012	0.004
	ν_6	0.027	1.000	0.002	0.000	0.000
B_{2u}	ν_7	0.085	0.000	1.000	0.120	0.034
	ν_8	0.035	0.000	0.073	1.000	0.058
	ν_9	0.027	0.000	0.050	0.029	1.000
		381	255	142	83	
	ν_{10}	1.000	0.081	0.007	0.000	
	ν_{11}	0.044	1.000	0.019	0.235	
B_{3u}	ν_{12}	0.011	0.006	1.000	0.021	
	ν_{13}	0.019	0.248	0.006	1.000	